UNIVERSITY OF OKLAHOMA

GRADUATE COLLEGE

DEVELOPMENT AND CHARACTERIZATION OF INJECTABLE BIOCOMPATIBLE HYALURONIC ACID HYDROGELS FOR POTENTIAL BRAIN ANEURYSM BLOCKAGE AND VASCULAR REGENERATION.

A THESIS

SUBMITTED TO THE GRADUATE FACULTY

in partial fulfillment of the requirements for the

Degree of

MASTER OF SCIENCE

By

KEREN FRAISSARD
Norman, Oklahoma
2022

Downloaded from SHAREOK. Persistent Handle URL: https://hdl.handle.net/11244/335980

DEVELOPMENT AND CHARACTERIZATION OF INJECTABLE BIOCOMPATIBLE HYALURONIC ACID HYDROGELS FOR POTENTIAL BRAIN ANEURYSM BLOCKAGE AND VASCULAR REGENERATION.

A THESIS APPROVED FOR

THE STEPHENSON SCHOOL OF BIOMEDICAL ENGINEERING

BY THE COMMITTEE CONSISTING OF

Prof. Rebecca Scott - Chair

Prof. Michael Detamore

Prof. John Clegg

Prof. Marc Moore

© Copyright by KEREN FRAISSARD 2022

All Rights Reserved.

Acknowledgments

I would like to thank my committee, Dr. Detamore, Dr. Clegg, Dr. Moore, and especially my advisor Dr. Scott, for their support, their advice, and for giving me the opportunity to defend this thesis in biomedical engineering. Working with Dr. Scott and Dr. Moore has been a fulfilling experience that gave me invaluable knowledge. I can't thank you both enough for all your precious time and help.

I would like to thank the Department of Biomedical Engineering, the UROP grant, and Polytech Clermont for their financial support and for giving me the opportunity to participate in this research here.

I want to thank my teachers at Polytech Clermont, Dr. Roche, Dr. Audonnet, and Dr. Delattre, for their help that allowed me to come here.

I also would like to thank Braden Barlean, my partner in this project, who dedicated his time and energy to the completion of this research. I am very grateful for all the help Dr. Kiyotake and Vinit Sheth gave us.

I also want to thank Ms. Glover, Ms. Hudson, and Ms. Hurley for their help with the paperwork. I would not have been able to graduate without your answers to my constant administrative questions.

I want to thank Coline Furrer for all her support from day zero. I couldn't have come here without you.

Finally, I want to thank my family for believing in me and supporting me. I love you.

Table of Contents

Abstract ix
Chapter 1: Motivation and literature review 1
1.1 Overview 1
1.2 Properties of brain blood vessels 2
1.2.1 Blood vessel structure 2
1.2.2 Composition of blood vessels 3
1.3 Brain aneurysm formation and aneurysm types 5
1.4 Current treatments 8
1.4.1 Surgical clipping 9
1.4.2 Coiling 10
1.4.3 Stents 11
1.4.4 Liquid fillers 15
1.5 Conclusion & Clinical Need 16
Chapter 2: Novel method for potential aneurysm treatment 18
2.1 Introduction and treatment characteristics 18
2.1.1 Potential wound repair and resorption of HA 20
2.1.2 Safe crosslinking and photo-initiating 21
2.1.3 Easy and safe imaging 23
2.2 Materials & Methods 25
2.2.1 Materials 25
2.2.2 PHA synthesis 26
2.2.3 PHA structural analysis 26
2.2.4 PHA hydrogels formation 27
2.2.5 Viscosity and flow 28
2.2.6 Mechanical testing 28
2.2.7 Swelling capacity 28
2.2.8 Tantalum visibility in hydrogels 29
2.2.9 Cell upkeep 30
2.2.10 Cell assays 30
2.2.11 Live dead assay 31
2.2.12 Statistical analysis 31
2.3 Results 32
2.3.1 Characterization of PHA 32
2.3.2 Viscosity of PHA solutions 33

2.3.3 X-rays to assess tantalum visibility 35
2.3.4 Mechanical properties of hydrogels 37
2.3.5 Swelling Capacity 39
2.3.6 Cell Viability 41
2.4 Discussion 42
Chapter 3: Conclusions and recommendations 48
3.1 Conclusions 48
3.2 Recommendations 49
References 51

List of Figures

Figure 1: Anatomy of a human artery 2
Figure 2: Structural modifications in the tunica intima at an arterial bifurcation 7
Figure 3: Main brain aneurysm types 8
Figure 4: Representation of a surgical clip on a saccular aneurysm neck 9
Figure 5: Representation of the insertion of a coil in a saccular aneurysm 10
Figure 6: Representation of a stent 12
Figure 7: Representative schematics depicting stent types 13
Figure 8: Method of insertion of a liquid filler 16
Figure 9: Injection method and functioning of our material 19
Figure 10: Formation of PHA 32
Figure 11: 1H-NMR for PHA Characterization 33
Figure 12: Viscosity and capacity to go through a catheter of our 40 kDa PHA/Tantalum material 34
Figure 13: Tantalum visibility in dental X-rays depending on tantalum concentration and cover on top of PHA 36
Figure 14: PHA hydrogels formation 37
Figure 15: Mechanical characterization of 40 kDa 5 wt%, 7.5 wt%. and 10 wt% PHA hydrogels with absence or presence of tantalum powder 38
Figure 16: Water absorption of 40 kDa 5 wt%, 7.5 wt%. and 10 wt% PHA hydrogels with absence or presence of tantalum powder 39
Figure 17: Swelling ratio of 40 kDa 5 wt%, 7.5 wt%. and 10 wt% PHA hydrogels with absence or presence of tantalum powder 40
Figure 18: Cell viability of human umbilical vein endothelial cells after 24 hours in contact with PHA hydrogel-soaked medium 41

List of Tables

Table 1: Comparison of brain aneurysm treatments 17
Table 2: Concentrations of tantalum as an imaging agent found in the literature 24

Abstract

Brain aneurysms are blood vessel wall deformations that affect 240 million people worldwide and their rupture causes the death of a fourth of the patients each year. Current brain aneurysm treatments, like surgical clips or coils, allow only partial aneurysm occlusion and partial blood vessel wall reconstruction. These treatments stay in the patient ad vitam, thus having a high risk of causing vessel wall inflammation. To address these issues, our approach is catheter-based delivery of an injectable, hyaluronic acid-based material that is compatible with radiographic and magnetic resonance medical imaging techniques. This material can be used to plug saccular brain aneurysms and induce vascular regeneration. To make our PHA hydrogels visible via brain imaging techniques to assess correct delivery and provide a control of the aneurysm degradation overtime, 50 mg/mL of tantalum powder (Ta) was incorporated to PHA hydrogels. To assess whether PHA hydrogel matches the compressive resistance of vessel walls, compressive moduli of 5, 7.5, and 10% PHA hydrogels without or with 50 mg of Ta per g of PHA were measured. The compressive moduli of 5, 7.5, and 10% PHA hydrogels without or with 50 mg of Ta per g of PHA increased with weight percent and were comprised within a 50 to 100 kPa range, which is the range of brain tissues' compressive moduli. To verify the biocompatibility of PHA hydrogels with blood vessels, the cell viability of human umbilical vein endothelial cells (HUVEC) in contact with medium infused for 24 hours with 5, 7.5, and 10% PHA hydrogels without or with 50 mg of Ta per g of PHA was quantified. The viability of HUVEC exposed to 5, 7.5, and 10% PHA hydrogels without or with 50 mg of Ta per g of PHA was a 100%. These data point out that injectable 5 and 7.5% PHA hydrogels with compressive moduli similar to brain tissues and good viability with endothelial cells can be made to potentially plug brain aneurysms.

Chapter 1: Motivation and literature review

1.1 Overview

Around 240 million people worldwide and 6.5 million in the United States (US) live with at least one unruptured brain aneurysm[1,2]. Moreover, approximately 6,500 Americans have aneurysms rupture each year, with half resulting in death because of brain hemorragies[2]. Popular treatments like coils and surgical clips efficiently seal aneurysms but they are costly, and they do not systematically make aneurysms disappear[3,4]. Moreover, many patients need second interventions because of aneurysm rupture or displacement of the treating tool, which increases the already-high costs[2,3].

To address these issues, our novel approach is catheter-based delivery of an injectable, biodegradable, hyaluronic acid-based material that is compatible with radiographic and magnetic resonance medical imaging techniques, that can be used to plug saccular brain aneurysms and induce vascular regeneration.

This introductory chapter describes the anatomy of brain blood vessels and aneurysms, and current treatments for brain aneurysms. Then, components of our novel hyaluronic-based biomaterial are discussed, including how it improves upon current treatments.

1.2 Properties of brain blood vessels

1.2.1 Blood vessel structure

Brain vessels consist of 3 layers that provide both elasticity and rigidity and which are, from inner to outer, the tunica intima (which includes the internal elastic lamina), the tunica media and the tunica adventitia (Figure 1)[5,6]. The structure of brain vessels is different from extracranial vessels because the former have a thinner layer of smooth muscle cells constituting their tunica media and are surrounded by cerebrospinal fluid instead of connective tissue[7].



Figure 1: Anatomy of a human artery. Hematoxylin and Eosin staining of a transverse section of a human artery. The A: tunica intima; B: internal elastic lamina; C: tunica media; D: external elastic lamina E: tunica adventitia are observed. Image taken using an optical microscope with a 20x objective of a Ward's Science slide, ref 470182-752. Scale bar = 0.03 mm.

1.2.2 Composition of blood vessels

Blood vessels, which are composed of cells and structural proteins, are divided into three main layers: tunica intima, tunica media, and tunica adventitia. The tunica intima is the inner layer of blood vessels. This lamina is composed of a layer of endothelial cells on a foil of proteins and macromolecules called the basement membrane[8]. These endothelial cells - also called the endothelium – minimize the friction with blood and are covered by the glycocalyx, which is an ensemble of proteoglycans, glycoproteins, and glycosaminoglycans[9,10]. The glycocalyx protects the endothelial cells and mediates their interaction with blood cells and their permeability to water and macromolecules[5,6]. Exterior of the tunica intima lays the tunica media, which is composed of a layer of smooth muscle cells[7]. The proteins of the glycocalyx also relay the changes in shear pressure and stress to the smooth muscle cells layer, which adjust their structure to the pressure, resulting in changes in the internal diameter of the vessel[10]. The tunica adventitia is mainly composed of fibroblasts that produces growth factors to regulate cellular growth and inflammatory response [11].

Many proteins and glycosaminoglycans are interspersed within the cell layers of the vessel. The main proteins found in the vascular wall are collagen, elastin and fibronectin[8]. Hyaluronic acid, a glycosaminoglycan, is also a major component of different parts of blood vessels. For example, in the smooth muscle cell layer, hyaluronic acid forms a scaffold for white blood cell adhesion[12], while in the glycocalyx, hyaluronic acid provides structure to endothelial cells and facilitates

vascular permeability[10]. Fibronectin is found in the basement membrane and in the tunica adventitia of blood vessels. Fibronectin proteins form a network that regulates the accumulation of other proteins, such as collagen types I and III[8]. Elastin is primarily localized to the tunica media and is the principal component of the elastic laminae, which gives structure and elasticity to the vessel wall[8]. Vascular structural proteins can also vary in composition depending on the function and localization of the vessel[5,8]. For example, the primary collagen types encountered in brain arteries are collagen III, IV and VI[13]. However, the specific composition varies depending on the type of cerebral arteries. For example, Dong *et al.*[14], studied the brain of 6 middle aged deceased subjects and demonstrated that collagen I is predominant in the tunica adventitia and intima of leptomeningeal arteries, while collagen III is moderately present in the tunica adventitia. Conversely, in grey and white matter capillaries, collagen III was present in relatively high quantities but collagen I was only faintly present and only traces of collagen IV found[14].

1.2.3 Mechanical properties of and experienced by blood vessels

Blood vessels both exhibit mechanical properties and undergo mechanical forces under physiological conditions. The tensile modulus of human brain arteries is approximately 21 MPa and the one of human brain veins is approximately 2.3 MPa[15,16]. This huge difference in tensile modulus between arteries and veins is due to the different percentage of elastin, which is greater in arteries[15]. Compressive modulus of brain

arteries is approximately 10 MPa whereas the compressive modulus of brain veins is around 4 MPa.[17]

The walls of blood vessels also undergo many types of mechanical constraints, including shear stress. Wall shear stress and shear pressure in brain arteries have been assessed by mechanical testing or 3D simulation. Kulscar *et al.*[18] studied three women between 44 and 58 and reported that their average shear stress of brain arteries was 10 Pa. Xiao *et al.*[19] found that shear pressure in brain arteries is in average 180 Pa in healthy brain arteries and 160 Pa in arteries presenting brain aneurysms.

1.3 Brain aneurysm formation and aneurysm types

1.3.1 Brain aneurysm formation

An aneurysm is a deformation of blood vessels, where a bulge forms due to weakening in the vessel wall. Aneurysm formation starts with accelerated blood flow[20,21], which may be caused by smoking, hypertension, and/or flow constraints at an arterial bifurcation, leading to high wall shear stress [7,20,21]. Indeed, during the formation of brain aneurysms, wall shear stress is at least 5 fold greater than the average wall shear stress of healthy brain arteries (around 40 to 60 Pa), according to Kulscar *et al*[18]. Wang *et al.*[22] found that in cerebral aneurysms, artery wall shear stress is lower than in healthy arteries, around 0.2 Pa in brain carotid artery[22]. Another study found that wall shear stress is 1.5 folds higher in healthy brain arteries than in aneurysms (6 Pa in aneurysms and 9 Pa in health artery) but found no difference in shear pressure (between 106 and 220 Pa in aneurysms and

between 104 and 270 Pa in health arteries)[19]. A third study found a low wall shear stress in cerebral aneurysms at arteries between 0.76 and 2.55 Pa[23]. These data, though statistically significant, however, come from 3D reconstructed aneurysm models and not in vivo data[19,22].

Abnormally high blood flow leading to increased vessel wall shear stress in blood vessels triggers collagen and extracellular matrix (ECM) reconstruction by smooth muscle cells (SMCs) and endothelial cells[7,20]. The first step of restructuring is the detection of increased wall shear stress by the glycocalyx, a network of glycoproteins and proteoglycans coating the endothelium[9], which triggers the release of macrophage chemotactic protein-1 (MCP-1). MCP-1 then recruits macrophages, which release cytokines and matrix metalloproteinases[21]. Among the former, interleukin 1β (IL-β) participates in blocking collagen synthesis, while tumor necrosis factor-β (TNF-β) induces SMCs to migrate to the tunica intima and contributes to the activation of matrix metalloproteinases (MMPs) released by macrophages[7,20,21].

As a result of these events, SMCs are disjointed[21], collagen fibers are reoriented, and the tunica intima thins (Figure 2). Collagen fibers are reoriented because collagen type changes, from mainly types III, IV and VI to mostly types I and V[7,20]. Aneurysm growth occurs after these structural changes because collagen fibers extend thanks to their reorientation[20]. Frösen *et al.*[20] presented aneurysm growth as inflammation driven: macrophages produce growth factors like TGF-β, which facilitate smooth muscle cells growth and simultaneously, through a series of immune mechanisms, recruit more macrophages, thus

maintaining inflammation, smooth muscle cell dysregulation, and ultimately, aneurysm growth.

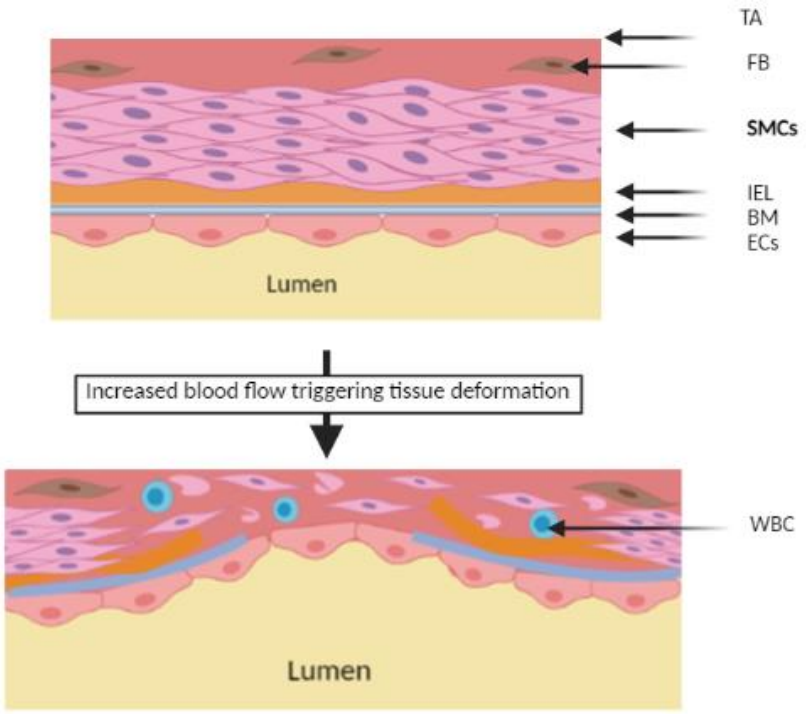


Figure 2: Structural modifications in the tunica intima at an arterial bifurcation. (Top) In healthy blood vessels, the tunica adventitia (TA) contains fibroblasts (FB) and lays on the tunica media which contains organized layers of smooth muscle cells (SMCs). The medial layer itself sits on the tunica intima which is composed of the internal elastic lamina (IEL), a basement membrane (BM) and an organized layer of endothelial cells (ECs). (Bottom) When increased blood flow triggers tissue deformation, it damages the basement membrane, the internal elastic lamina and the smooth muscle cells. The cellular debris recruits immune cells (WBC) that start inflammation, which will drive aneurysm growth.

1.3.2 Types of cerebral aneurysms

When cerebral aneurysms are fully formed, different types can be observed (Figure 3). Aneurysms are generally comprised between 5 and 10 mm[24]. Micro (Figure 3A) and giant (Figure 3B) aneurysms are characterized by their size which measure less than 2 mm and more than 25 mm, respectively[2,25]. Saccular (Figure 3C) and fusiform (Figure 3D) aneurysms are defined by their location at the bifurcation of an

artery. Saccular aneurysms are like pockets that can be distinguished from the vessel core, whereas fusiform aneurysms are swellings within the vessel. The position of the aneurysms allows them to relocate thinner vessels to fuel the aneurysms[25], such as how tumor-mediated stimulation of angiogenesis[26].

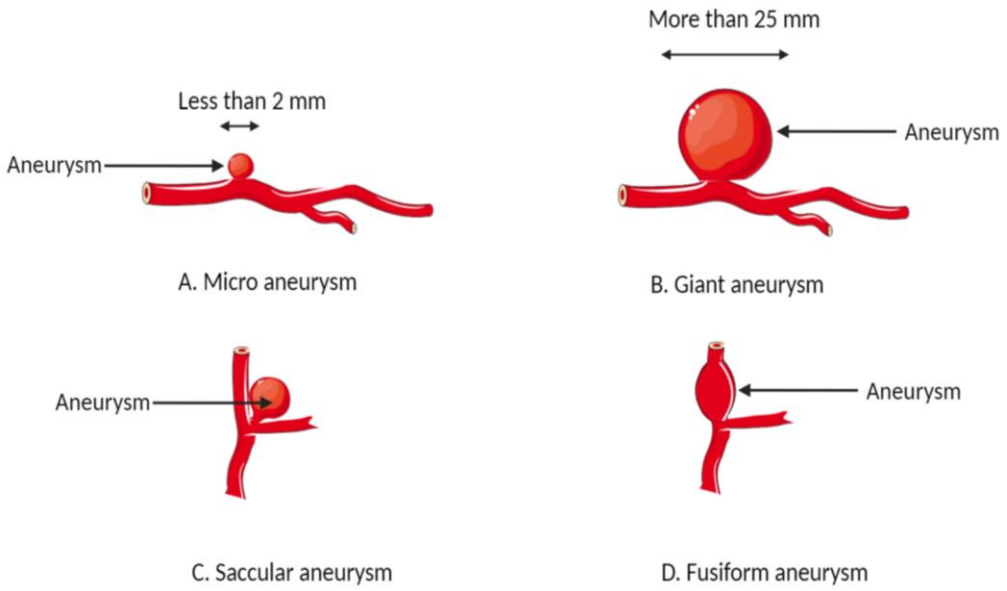


Figure 3: Main brain aneurysm types. Aneurysms are classified based on their locations and sizes. Normal aneurysm size is between 2 mm and 25 mm in diameter. (A) Under this threshold, they are defined as micro aneurysms, while (B) giant aneurysms fall above. (C) Aneurysms located at bifurcations of blood vessels, but outside the vessel, are denoted as saccular aneurysms. (D) Aneurysms at bifurcations of blood vessels, but located inside one of the branches of the bifurcation, are named fusiform aneurysms.

1.4 Current treatments

The current aneurysm treatments are medical devices that are place inside or around the neck of the aneurysm to stop blood from flowing inside aneurysms and prevent aneurysm rupture. The most used treatments include surgical clips, coils, stents, and liquid fillers, which are discussed below.

1.4.1 Surgical clipping

Surgical clipping requires an open skull surgery to access and block the aneurysm with a clip, which restores normal blood circulation in the main vessel (Figure 4). Patients treated with surgical clips have high survival rates. For example, in the United Kingdom (UK) cohort of an international subarachnoid aneurysm trial, Molyneux *et al.*[4] reported that, 10 years after surgical clipping, 79% of the 835 patients were alive. In addition, clipping is suited to most brain aneurysms types[25] and patients can be treated even if their aneurysm is ruptured[27]. In a study by Raper *et al.*[27], six patients who were initially treated with coils had aneurysm ruptures, but surgical clipping fully closed these ruptured aneurysm necks.

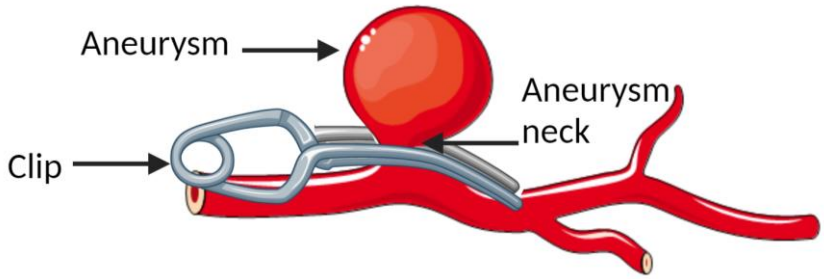


Figure 4: Representation of a surgical clip on a saccular aneurysm neck. The surgical clip pinches the aneurysm neck to prevent blood from going in the aneurysm and causing aneurysm rupture.

Unfortunately, surgical clipping can be expensive. For example, the average cost of the clipping procedure in the US was $24,000 in 2008[3]. In a 20-year cost comparison of surgical clipping procedures, Engele *et al.*[28], found that clipping costs are hospital-dependent, vary between $20,000 and $80,000, and can be up to 30% more expensive than coiling[28]. Moreover, clipping requires an open surgery of the skull,

which increases chances of complications[29]. Hoffman *et al.*[30] studied 7036 patients, half of the patients were treated with coils and the other half with clips, finding that patients with clips were 20% more likely to be readmitted at the hospital, 90 days after treatment, than patients with coils[30]. In summary, clips have a high successful aneurysm closure rate, even in patients with ruptured aneurysms, and are suited to most aneurysm types. However, clips are expensive, require an invasive surgical procedure, and may result in a higher readmission rate.

1.4.2 Coiling

Coiling is a minimally invasive aneurysm treatment that consists in inserting a wire-containing catheter, also known as a coil, in a vessel near the aneurysm and coiling the wire to fill the aneurysm[31] (Figure 5). To reinforce the vessel wall, stents can be inserted along with coils (see

1.**4.3 Stent** subsection below)[25]. Stents are often inserted before coils, because they help in the process of coiling within complex giant and fusiform aneurysms[25].

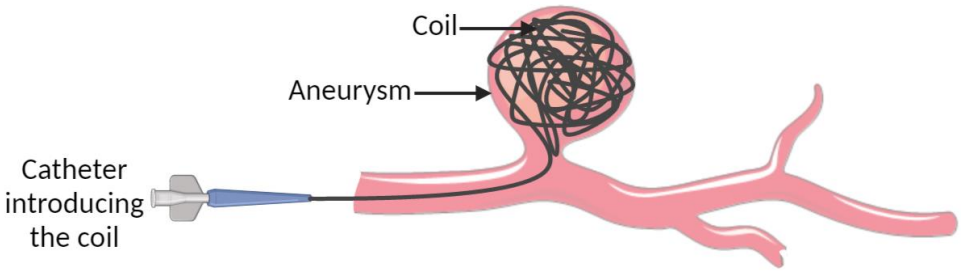


Figure 5: Representation of the insertion of a coil in a saccular aneurysm. A micro catheter is inserted in a patient blood vessel to deploy and coil (a wire) into the aneurysm to prevent blood from flowing inside the aneurysm.

Coiling is efficient and less invasive than surgical clipping. The International Subarachnoid Aneurysm Trial recorded the recovery rates of 2,143 patients with coils or stents-treated aneurysms[4]. In the UK cohort of this trial, Molyneux *et al.*[4] observed that, 10 years after surgical clipping, 83% of the 809 patients were alive. In a similar study conducted in the United States, Hoffman *et al.*[30] recounted that of 8,564 patients, with half treated with coils and half with clips, those treated with coils had less severe 30-day readmission issues than patients treated with clipping. Unfortunately, costs for coiling procedures are high and vary across hospitals and regions. Engele *et al.*[28] compared coiling and clipping costs during 20 years at various locations in the US, and found that while coiling is 10 to 30% less expensive than clipping, coling prices can vary from $13,000 to $83,000. Moreover, coils can also induce thrombosis, blood clot formation, and inflammation[32]. Taken together, coiling is a minimally invasive procedure that has a good aneurysm closure success rate, but it is expensive and can cause inflammation and blood clot formation.

1.4.3 Stents

A stent is a medical device shaped as a tube and made of a network of wire (Figure 6). Stents are mostly used for stent-assisted coiling; however, covered stents can be used on their own to treat aneurysms[25]. Stents are inserted in patients the same way coils are: a microcatheter is introduced in a vein or artery up to the aneurysm location, where the stent is deployed through expansion of a balloon at the end of the microcatheter[33]. Stents allow aneurysms to disappear due

to the gradual formation of a blood clot in the aneurysm, on the surface of the stent. The combination of the clot and the mesh of the stent support the formation of new tunica intima layer and then the reconstruction of the vessel walls[32]. In general, stenting is an effective procedure, with a previous study reporting that 70% of patients had a complete occlusion of their aneurysm after a year and 92% of patients had 90% of their aneurysm occluded after a year[33]. However, this procedure often requires taking anticoagulant medication to fluidify blood to prevent blood clot formation[33]. In an American study on 153 patients, Fiorella *et al.*[33] reported that subjects were administered an anticoagulant a week before the procedure and at least 3 months after the procedure or *ad vitam aeternam,* as needed.

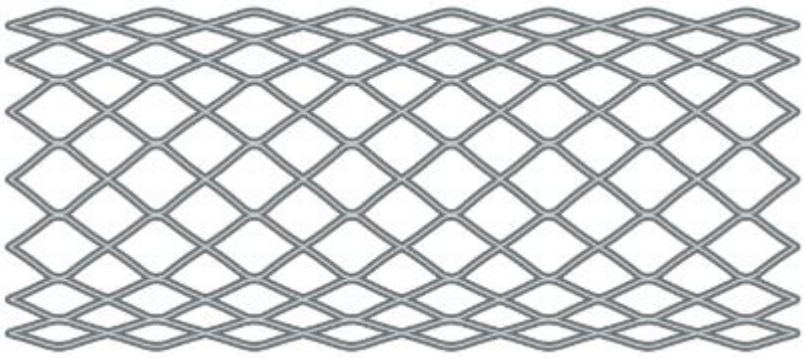


Figure 6: Representation of a stent. A stent is a medical device made of a network of metal wires.

As mentioned previously, there are many clinical procedures that combine the use of stents and coils to heal aneurysms (Figure 7). The best-known technique is called stent jail coiling (Figure 7A). This technique consists in inserting a stent using a microcatheter, removing the catheter, and then inserting a coil with another microcatheter. However, when the microcatheter for coil deployment is removed, there

is a risk of accidentally moving the stent. To solve this, another technique called semi-jailing (Figure 7B) is used. In this method, the stent is only half deployed prior to insertion of the coil. After the coil's microcatheter is removed, the stent catheter is fully deployed[34].

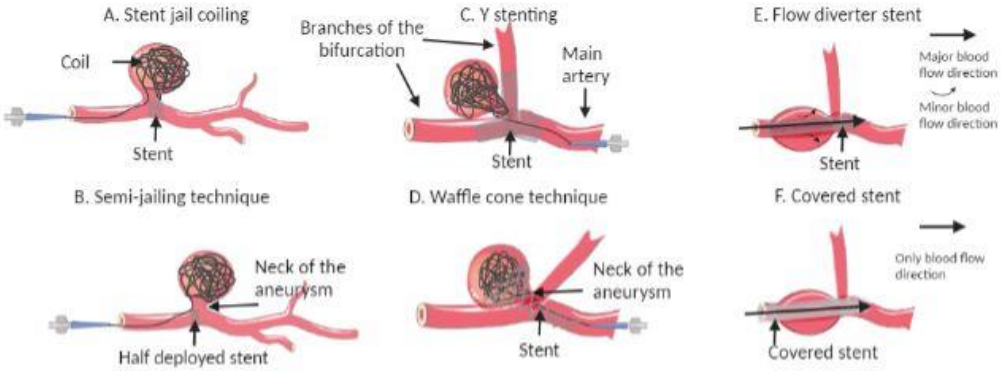


Figure 7: Representative schematics depicting stent types. A: Stent jail coiling: a stent is deployed with a microcatheter, then a coil is inserted. B: Semi-jailing technique: a stent is half deployed with a microcatheter, then a coil is inserted, and finally the stent is fully deployed. C: Y stenting: two stents are inserted in the main artery and through each branch of the bifurcation, and then is inserted a coil that leans on them from inside the aneurysm. D: Waffle cone technique: a stent is deployed from the main artery to the neck of the aneurysm and then a coil is inserted in the aneurysm and leans on the stent. E: Flow diverter stent: a stent is deployed through the aneurysm. F: Covered stent: a stent covered by expendable polymers is deployed through the aneurysm.

Another stenting method, called the Y-stenting technique (Figure *7*C), is used for intracranial aneurysms located at bifurcations. As the main vessel splits into two branches at a bifurcation, two stents are inserted into the main vessel in this method, where one stent is placed in the main vessel and another in one branch of the bifurcation. Then, at least one coil is inserted in the neck of the aneurysm and the coil lies on the two stents[35]. Unfortunately, the Y technique is not appropriate for wide-neck aneurysms at bifurcations. As such, the waffle cone technique

(Figure 7D) is used. For the efficiency of this method, the maximum diameter of the stent must be larger than the neck of the aneurysm. Compared to the Y technique which uses two stents, the waffle cone only uses one, which reduces the risks of thrombosis and stenosis (blood clot formation and vessel narrowing)[36], but the technique requires a high dexterity to correctly position the stent[25].

For fusiform aneurysms, which are located at bifurcations but are in the main artery or vein and thus, cannot be treated with the Y stenting technique, flow diverter stents (Figure 7E) are utilized. Flow diverter focus and direct the blood flow in a straight line, while reinforcing the vessel wall[25]. Covered stents (Figure 7F) are a subgenre of flow diverter stents that are covered by a layer of expendable polymer as polyurethane[37] or expanded polytetrafluoroethylene[38]. This polymer layer completely prevents the blood from flowing in the aneurysm and, compared to the uncovered network of wires of flow diverter stents, reduces the risk of blood clot formation[25].

Stent-assisted coiling allows for treatment of brain aneurysms in intracranial locations including at the basilar trunk, middle cerebral arteries, or carotid bifurcations[33]. One of the most difficult locations in which a stent can aid in the treatment of a brain aneurysm is around the circle of Willis, which is a strategic point of brain blood circulation as four of the main brain arteries are joined there[39]. Repairing the vasculature in this location is crucial for maintaining brain tissue integrity[39]. In a study of 25 patients with aneurysms on arteries of the circle of Willis, Schob *et al.*[32] used 0.017 inch microcatheters to deliver stents and coils in

proximal and distal segments of Willis's Circle arteries in fusiform and saccular aneurysms. After 3 months, 63% of aneurysms were fully occluded and 85% were partially occluded[32].

Taken together, stents are minimally invasive and reinforce blood vessel walls either alone or to enable coiling in a wide range of aneurysm types that may not be candidates for treatment by clipping or simple coiling. However, stents can require taking anticoagulant medication, can cause inflammation or thrombosis, stay forever in the patients, and for most stent types, do not totally heal nor rebuild the blood vessel wall[25,32].

1.4.4 Liquid fillers

Liquid fillers, or embolic agents, are liquid polymers mixed with imaging agents, which allow the procedure to be monitored by angiography. The mix is inserted into aneurysms through catheters and spontaneously solidify in contact with blood[40]. Similar to coiling, this technique does not require open surgery of the skull and uses standard tools as a balloon catheter to block blood flow and a microcatheter to insert the embolic agent (Figure 8). Unlike coiling, liquid fillers can fit asymmetrical aneurysms thanks to their liquid state[25]. The most studied liquid filler is the Onyx embolization agent by Medtronic. Onyx is composed of ethylene vinyl alcohol copolymer for aneurysm filling, DMSO for polymer solubilization, and tantalum powder for imaging[41]. Several small clinical studies have been conducted with Onyx. For example, Chalaoui *et al.*[42] found that 13 out of 16 patients had a successful occlusion of their aneurysm, including patients with ruptured

aneurysms. Another study reported that liquid fillers do not cause inflammation and thrombosis, contrary to coils[43]. However, one major risk of embolization agents is the potential of filler fragmentation by blood flow[40].

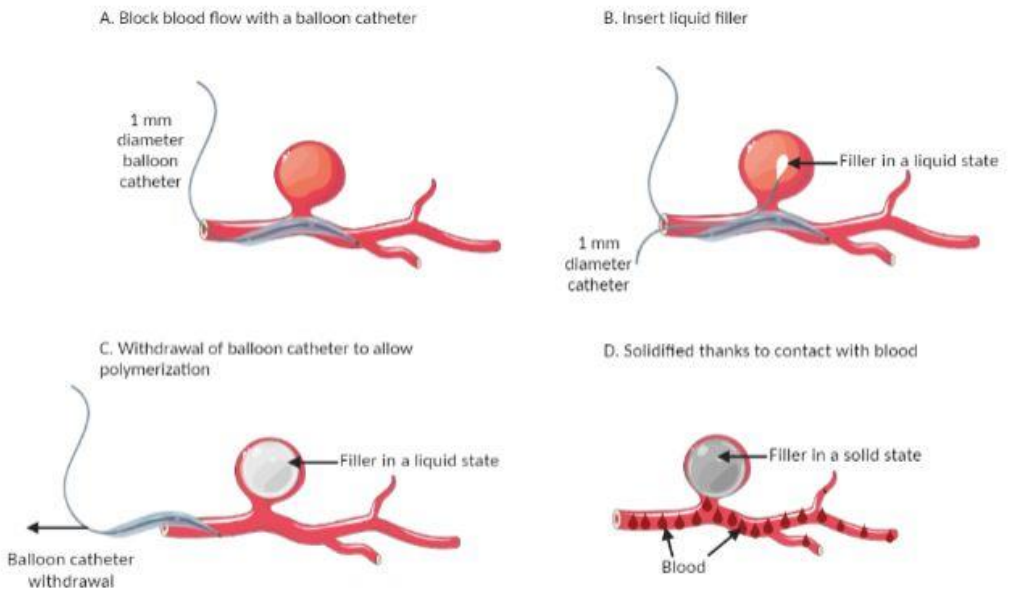


Figure 8: Method of insertion of a liquid filler. A: A balloon catheter is inserted to block the blood flow. B: The filler, in its liquid state, is injected with a microcatheter. C: The balloon catheter is withdrawn, which enables the blood to flow back into the vessel. D: When the liquid filler enters in contact with blood, it solidifies.

1.5 Conclusion & Clinical Need

Cranial aneurysms are deformations of brain blood vessels that form because of increased blood flow pressure[7,21] and if left untreated, can rupture and lead to death.

Table 1: Comparison of brain aneurysm treatments

Treatment Name	Success Rate	Drawbacks	Advantages	Referen-ces
Surgical Clipping	78% of 1,000 patients at 10 years did not undergo brain or motor function damages after surgery	- Of 7,000 patients, 20% more 90 days readmission than coiling - Open skull surgery - Blood vessel wall is not rebuilt	- Available for many aneurysm types - Better than coil to stop hemorrhages definitely	4,25,27,30
Coiling	82% of 1,000 patients at 10 years did not undergo brain or motor function damages after surgery	- Can cause inflammation or thrombosis - blood vessel wall is not rebuilt	- Minimally invasive	4,25,30,43
Stent Assisted Coiling	92% of 153 patients had a 90% aneurysm occlusion after a year	- Can require taking anticoagulan t medication - Can cause inflammation or thrombosis - blood vessel wall is not rebuilt	- Minimally invasive - Support the reconstructio n of the vessel wall	32,33
Liquid Fillers	81% of successful aneurysm blockage (16 patients)	- Risk of fragmentatio n by blood flow - Recent so do not have success rates over time	- Minimally invasive - Do not cause inflammation or thrombosis - Adapted to asymmetrical aneurysms	25,40,43

Current treatments allow partial vessel wall reconstruction and stop aneurysm growth by blocking the blood flow from going in the aneurysm, but either require open skull surgery, can cause thrombosis and inflammation, or can be fragmented by blood flow (Table 1) [28,31,33,42]. Thus, there is a need for a minimally invasive treatment that does not cause inflammation, that promotes wound repair, and is safely resorbed by the body. In this work, we propose a novel solution, that is noninvasive, non-cytotoxic, angiogenesis enhancing and resorbable, which will provide an improved solution to treat brain aneurysms.

Chapter 2: Novel method for potential aneurysm treatment

2.1 Introduction and treatment characteristics

Previously, we established the characteristics of an ideal treatment for brain aneurysms, which include being safe and biocompatible, inducing wound regeneration and angiogenesis, being resorbable, being visible with non-invasive imaging techniques to provide follow-ups, and being minimally invasive. As such, our own solution, which is depicted in Figure 9, is inspired by these characteristics. Briefly, our treatment will be introduced in patients as a liquid, via a 1 mm thick catheter, after blocking blood flow in the vessel at the site of the aneurysm with a balloon catheter. The liquid solution, comprising pentenoate hyaluronic acid (PHA), dithiothreitol (DTT) as the crosslinker, lithium phenyl-2,4,6 trimethylbenzoylphosphinate (LAP) as the photo-initiator, and phosphate buffered saline (PBS), will then be

safely crosslinked in the aneurysm with 365 nm UV light delivered through a 1 mm thick pigtailed diode catheter. The whole process is expected to take between 5 and 8 minutes and is applicable to aneurysms with a 1.5 dome to neck ratio, which means that, optimally, the diameter of the aneurysm must be one and a half times wider that the diameter of the aneurysm neck. Resorption will be tracked by imaging with x-ray tomography by tracking the tantalum powder added in the hydrogel material.

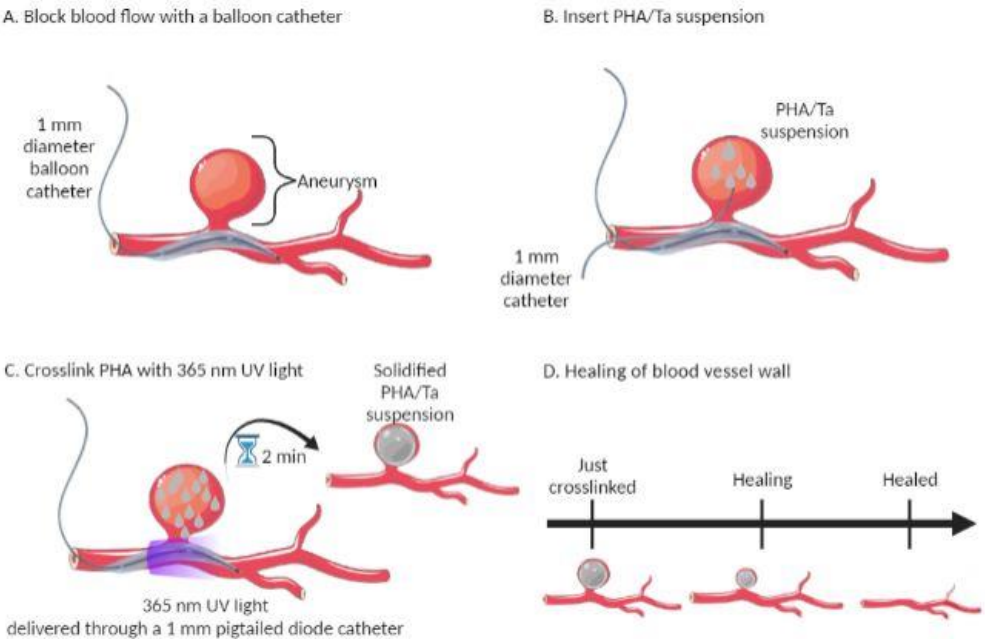


Figure 9: Injection method and functioning of our material. PHA/Ta: our material made of pentenoate hyaluronic acid and tantalum powder. A: First, a balloon catheter is inserted in the main vessel to prevent blood from flowing in the aneurysm. B: Then, a microcatheter is used to inject the PHA in its liquid state. C: PHA is crosslinked with a 365 nm UV light for two minutes to form a hydrogel. The balloon catheter is withdrawn. D: Because the aneurysm is not fueled by blood, it dies over time and as it degrades, the PHA degrades with it while enhancing blood vessel reconstruction.

Finally, our HA-based material favors wound repair and angiogenesis and is expected to be safely resorbed, in theory within 28

days[44,45]. In the following sections, the choice of our materials will be justified.

2.1.1 Potential wound repair and resorption of HA

Our goal is to treat aneurysms by introducing a material within the aneurysm that isolates the aneurysm from blood flow and promotes aneurysm resorption and regeneration of the vessel wall. Hyaluronic acid (HA) was chosen because previous studies showed that HA is degradable and promotes wound healing. You *et al*.[44] utilized hydrogels consisting of one layer of poly lactide-co-glycolide mixed with HA hydrogels between two layers of 5 weight percent (wt%) or 10 wt% HA to fill ruptured bones and demonstrated that in 28 days the 3-layer hydrogels were fully resorbed. Similarly, Hertegård *et al*.[45] made hyaluronic acid hydrogels to help wound regeneration, and noticed total HA resorption after 25 days.

Deng *et al.*[46] used chitosan and hyaluronic acid hydrogels to repair abdomen wounds in rabbits. The authors noticed wounds treated with the hydrogels exhibited an increase in cytokines that promote angiogenesis, a 2.5-fold increase in thickness of newly formed tissues compared to wounds without hydrogel, and activated M2 macrophages, which indicates fibrogenesis. Hong *et al.*[47] observed the scaring rates of rabbits wounds covered with HA hydrogels. After 14 days, wounds covered by hyaluronic acid hydrogels were 58% smaller than at day one, whereas wounds without it were, at day 14, only 28% smaller than day 1. Supporting this observation, the authors found the presence of transforming growth factor beta-1 (TGF-β1), which starts the skin healing

procedure, at day 7 in the wound with hyaluronic hydrogels; however, this growth factor was not observed in control wounds (i.e., wounds without hydrogel) until day 14. Ghose *et al.*[48] studied the effects of HA on the proliferation of endothelial cells from livers of mice. They noted that endothelial cells with 10 mg/mL of HA grow in 48 hours two times faster than endothelial cells alone. They also quantified angiogenic factors expression in 48 hours of these endothelial cells with 10 mg/mL of HA and observed an increase of by 4-fold, 7-fold, and 8-fold with HA compared to control, of vascular endothelial growth factor, catenin β, and vascular endothelial growth factor receptor 1, respectively[48].

The literature above shows that HA is a resorbable polymer that promotes wound healing. On one hand, it will be a good material to enhance wound healing of the vessel wall at the neck of the aneurysm. On the other, HA will be an appropriate material because it will be resorbed along with the aneurysm.

2.1.2 Safe crosslinking and photo-initiating

Our treatment will be injected into an aneurysm as a liquid solution of PHA. Thus, once PHA is delivered in the aneurysm, to solidify is with UV light, a photo-initiator – a chemical that reacts to UV light - is needed. Among all the photo-initiators, LAP was chosen for its low toxicity and low radical production, as justified by the studies below.

Fairbanks *et al.*[49] studied the effects of two combinations of LAP concentrations and exposure times to 10 mW/cm^2 of 365 nm UV light on human neonatal foreskin fibroblast. The combinations were 2.2 mM of LAP/ 1 min UV exposure and 0.22 mM LAP/ 10 min UV exposure. Cells

survival rates after 24 hours in contact with hydrogels (so with LAP and after UV exposure) were 95±2% and 96±2%, respectively. The first combination showed that standard concentrations of LAP are not harmful to cells, at least during the first 24 hours of contact. The second combination showed that cells can survive 10 min of exposure to 10 mW/cm^2 of 365 nm UV light without being damaged[49].

Nguyen *et al.*[50] found similar results by exposing human primary renal proximal tubule epithelial cells to solutions of 0.008, 0.04, 0.2, and 1 mg/ml of LAP and to 86, 342, or 855 mJ/cm^2 350-400 nm UV radiation. They noticed that the intensity of the UV light did not impact cell health but the growing concentrations of LAP did. While 0.008, 0.04, and mg/mL of LAP led to 92.5%, 85.4%, and 78.9% of cell survival, 1 mg/mL of LAP resulted in 67.1% of cell survival. Nguyen *et al.*[50] also investigated the liberation of NAD^+ radicals by the UV light activation of LAP, and concluded that it increased with LAP concentration and decreased with UV exposure intensity and wavelength. Apparently, an exposure of 855 mJ/cm2 of 350-400 nm UV light combined with 0.01 mg/mL of LAP release nearly 0% of radicals[50].

McCall *et al*.[51] specifically investigated the formation of radicals during 10 mW/cm2 365 nm crosslinking of LAP during 5 minutes. They reported that the concentration of acrylate radicals from 1 mM LAP was 1.82 mM and the concentrations of thiol-ene radicals from 0.1, 1, and, 10 mM LAP were respectively 0.11, 0.13, and 0.27 mM. Then they evaluated the impact of these radicals on several proteins as TGFβ,

lysozyme or collagenase 3, and concluded that at these 10^{-1} mM concentrations there was no bioactivity loss and no impact on cells[51].

These studies shed light on the good survival rates of cells in contact with LAP, which makes it an appropriate photo-initiator to start the crosslinking reaction of PHA into hydrogels.

2.1.3 Easy and safe imaging

Because PHA hydrogels are transparent, to non-invasively assess with X-rays that our treatment is properly injected in patients, an imaging agent is necessary. X-rays for brain imaging are safe and used in several procedures as fluoroscopy or computed tomography[52,53]. Fluoroscopy is a continuous imaging technique that uses X-Rays to provide images during a procedure. It is a well-known and FDA approved method which has various applications as blood vessel visualization, catheter insertion or stent visualization during aneurysm surgery[41,53]. Conlin *et al.*[52] used computed tomography of the brain of a patient to find the source of their headache.

There are many different possible biocompatible imaging agents for X-rays such as bismuth chelate[54], iodine, ferrous sulfate, tantalum, copper sulfate[55]. Roberts *et al.*[56] observed that tantalum (Ta) offers a better imaging contrast than iodine above 80 kVp, while Rathnayake *et al.*[57] reported that tantalum brings more contrast and details with dual contrast dual energy computed tomography, compared to bismuth. Moreover, tantalum was used in the Onyx embolization agent[41], which is a marketed product that aims to fill aneurysms, repair them and allow follow up by computed tomography imaging.

Table 2: Concentrations of tantalum as an imaging agent found in the literature

Contrast agent	Used in	Concentration	Reference
Carboxybetaine zwitterionic Tantalum oxide nanoparticles	Rat blood vessels	138 mg Ta/mL	[58]
Zwitterionic forms of tantalum oxide nanoparticles	Rat blood vessels	190 mg Ta/mL	[56]
Tantalum oxide nanoparticles	Rabbit blood vessels	240 mg Ta/mL	[59]
Tantalum oxide nanoparticles	Rabbit enteric blood vessels	16 mg Ta/mL	[57]

Tantalum's safety and biocompatibility has been evaluated in several studies. Roberts *et al.*[56] used tantalum oxide nanoparticles (injected in Lewis rats at 300 mg Ta/kg) as imaging agents and found that the total nanoparticle retention in naïve Lewis rats was 1.49% 48 hours post-injection, which shows that most of the tantalum injected gets out of the body after 2 days ; thus, tantalum does not pollute the body. Wang *et al.*[60] used porous tantalum as a bone replacement. The researchers demonstrated that tantalum in contact with osteoblasts for 8 days did not affect cell proliferation, and tantalum in contact with bones *in vivo* increased bone regeneration and collagen type I secretion.

Different tantalum concentrations found in the literature have been compiled in Table *2*. In blood vessels, most tantalum

concentrations used are around 200 mg of Ta per mL[56,58,59]. However, FitzGerald *et al.*[58] reported that the concentration of tantalum introduced was diluted by at least a factor 10 by the blood stream, so most concentrations are around 10 or 20 mg Ta/mL. Rathnayake *et al.*[57] reported using concentrations around 1 mg Ta/mL, in studies where blood dilution was not a factor. Due reports from previous literature, we plan to move forward with using 5 mg Ta/mL as a low concentration and 50 mg Ta/mL as a high concentration in our novel aneurysm treatment.

These studies show that X-rays can be used to safely image the brain. Tantalum powder is an imaging agent that will make PHA visible on X-rays, thus allow non-invasive monitoring of PHA injection in aneurysms.

2.2 Materials & Methods

2.2.1 Materials

Hyaluronic acid (HA; 40 kDa) was purchased from Lifecore Biomedical, Chaska, MN, United States. N,N-dimethylformamide (DMF; ≥99.8%), 4-(dimethylamino) pyridine, ≥99%, 1M sodium hydroxide (NaOH; ≥97.0%), 4-pentenoic anhydride 98%, sodium chloride (NaCl; ≥99%), acetone (≥99.5%), 3-(trimethylsilyl)propionic-2,2,3,3-d4 acid sodium salt, D_2O, tantalum powder (Ta; 60 to 100 mesh), dithiothreitol (DTT; ≥95%), and lithium phenyl-2,4,6 trimethylbenzoylphosphinate (LAP; ≥95%) were purchased from Sigma-Aldrich, Saint-Louis, MO, United States. Phosphate-buffered saline (PBS, 1X), Tween-20 (50% solution), and Triton X-100 were purchased from Thermo Fisher

Scientific, Waltham, MA, United States. Primary human umbilical vein endothelial cells (HUVEC; normal); HUVEC culture medium, and growth factors were purchased from ATCC, Manassas, VA, United States. Calcein-AM (4 mM in DMSO), Ethidium homodimer III (EthD-III; 2 mM in DMSO/H_2O), and AccuGreen DNA assay kit (including dye, buffer, and DNA standards) were purchased from Biotium, Fremont, CA, United States. Alamar blue dye was purchased from Bio-Rad, Hercules, CA, United States.

2.2.2 PHA synthesis

To create PHA, hyaluronic acid (1 g) was dissolved in 200 mL of DI water at room temperature. DMF was added to the water at a 2:3 ratio of DMF:DI water and stirred at 250 rpm until completely dissolved. Then, 250 mg of 4-(dimethylamino)pyridine were dissolved in the HA solution. Pentenoic anhydride (2.4 mL) was added in 10 times. The pH was the adjusted to pH 8-9 by addition of 1 M NaOH and stirred overnight at room temperature. NaCl (5 g) were dissolved in the HA solution. The solution was precipitated by addition of 2 L of acetone and centrifuged at 6,000 g for 3 minutes 3 times. The pellets were dissolved in DI water and dialyzed for 2 days in dialysis tubing (MWCO: 6-8 kDa, VWR, Radnor, PA). The pH of the solution was then adjusted to 7.4 with NaOH, lyophilized to dryness, and stored as a lyophilized powder at -20°C until use.

2.2.3 PHA structural analysis

PHA was dissolved in 3 mg/mL of D_2O. Then 1 mg/mL of 3-(trimethylsilyl)propionic-2,2,3,3-d4 was added and the solution was put

in a glass NMR tube. The sample was then run on an NMR 500 with the software VNMRJ (Agilent, Santa Clara, California). The NMR was tuned and shimmed, then a proton spectrum was collected and analyzed with the software MestReNova (MestReLab Research, La Coruna, Spain). The concentration mmol of pentenoate per gram of PHA was calculated with the following equation:

$$\frac{mmol\ pentenoate}{g\ PHA} = \frac{\int\ pentenoate}{\int\ TMSP} * \frac{9H}{1H} * \frac{mmol\ TMSP}{g\ PHA}$$

.

The concentration of mmol of pentenoate per gram of PHA is the integral of pentenoate divided by the quantity of PHA in the sample tested, to obtain the number of alkene chemical groups, standardized by the quantity of TMSP over the integral of TMSP.

2.2.4 PHA hydrogels formation

Lyophilized PHA was dissolved in PBS overnight at 4°C, to make 5 wt%, 7.5 wt% and 10 wt% PHA solutions. Meanwhile, a solution of 1.3 mg/mL LAP and 2 mg/mL DTT, dissolved in 1X PBS, was made and shielded from light. The PHA and LAP/DTT solutions were then combined 1:1 to create 5 wt%, 7.5 wt%, and 10 wt% PHA solutions. For hydrogels containing tantalum (Ta), Ta powder was added to the PHA/LAP/DTT solution to form solutions of 50 mg of TA per mL of PHA. Solutions were pipetted into a 1 mm thick rubber mold sandwiched between 2 glass slides and placed under a 365 nm UV light at 9 mW/cm^2 for 2 minutes to form hydrogels.

2.2.5 Viscosity and flow

Liquid PHA solutions (5 wt%, 7.5 wt%, and 10 wt%) were fabricated with the same protocol as PHA hydrogels but were not crosslinked. Viscosity was determined with a 40 mm cone with a 2° angle on a Discovery Hybrid Rheometer-2 (TA Instruments, New Castle, Delaware). Flow was evaluated by pushing liquid PHA solutions (5 wt%, 7.5 wt%, and 10 wt%) through a 1 mm diameter catheter, and qualitatively classifying them between “flow” and “no flow”.

2.2.6 Mechanical testing

PHA hydrogels (5 wt%, 7.5 wt%, and 10 wt%) were fabricated as described previously and punched out into 6 mm of diameter circles with a biopsy punch. Hydrogels were soaked in 1X PBS at 37°C overnight. Swollen hydrogels diameters were measured via a micrometer. Compressive elastic moduli were determined with 8 mm parallel plates on a Discovery Hybrid Rheometer-2 (TA Instruments, New Castle, Delaware) using a strain rate of 5 μm/s (~0.25% strain/s) until 20% strain and at 25°C, as described by Kiyotake *et al*.[61] Before each measure, a 0.1 N axial force was applied to ensure the hydrogel and instrument were in contact. The compressive elastic moduli were calculated for the portion of the slope where strain rates were 10 to 20%.

2.2.7 Swelling capacity

PHA hydrogels were fabricated as described previously and punched out into 6 mm of diameter circles with a biopsy punch. Fabricated weights were then recorded. Hydrogels were soaked in 1X PBS at 37°C overnight and then the swollen weights of the hydrogels

were recorded. Hydrogels were frozen at -20°C for 30 minutes, lyophilized overnight, and dry weights were recorded. The swelling capacity was estimated with two different parameters:

$$absorption = \frac{swollen\ weight\ [mg]}{fabricated\ weight\ [mg]}$$

$$swelling\ ratio = \frac{swollen\ weight\ [mg]}{dry\ weight\ [mg]}$$

Absorption and swelling ratio both indicate how much fluid PHA can absorb, though the swelling ratio gives a supplementary information on the absolute fluid intake of PHA from its dry for to its hydrogel form.

2.2.8 Tantalum visibility in hydrogels

To assess tantalum visibility within the hydrogels, dental X-rays of 10 wt% PHA hydrogels with and without 50 mg/mL of tantalum were taken with a Pro X dental X-ray unit (Planmeca, Finland). Images with hydrogels only, as well as hydrogels covered by 47 mm high ballistic gels (to simulate brain tissue) or hydrogels covered by 47 mm high ballistic gels and 4.8 mm thick PLA covers (to simulate both brain tissue and skull), were taken with an exposure time of 0.080 seconds, at 7 kV and 8 mA. The intensity of tantalum particles in hydrogels was quantify with ImageJ by analyzing the intensity of hydrogels per mm^2 with the following formula:

$$\frac{integrated\ density\ of\ PHA\ hydrogel}{area\ of\ hydroge\ in\ mm2} - \frac{integrated\ densited\ of\ background}{area\ of\ hydroge\ in\ mm2}$$

2.2.9 Cell upkeep

Human umbilical vein endothelial cells (HUVEC) were cultivated in vascular cell basal medium with the following endothelial growth factors (ATCC, Manassas, VA): 5 ng/mL of rhVEGF, 5 ng/mL of rhEGF, 5 ng/mL of rhFGF basic: 5 ng/mL, 15 ng/mL of rhIGF-1, 10 mM of L-glutamine, 0.75 Units/mL of heparin sulfate, 1 µg/mL of hydrocortisone, 50 µg/mL of ascorbic acid, and 2% fetal bovine serum. The cells were maintained at 37°C with 5% of CO_2 and 95% humidity. For all assays, cells were used between passages 7 and 9.

2.2.10 Cell assays

To create hydrogels for cell culture assays, lyophilized PHA was sterilized with ethylene oxide gas for a 12-hour cycle (AN74i, Anderson Anprolene, Haw River, NC) prior to solubilization. LAP and DTT were sterile filtered. Tantalum powder was sterilized in a sterilizer at °C for minutes. Under a biosafety cabinet, the sterilized PHA, LAP, DTT, and TA was crosslinked to form 5 wt%, 7.5 wt%, and 10 wt% hydrogels with and without 50 mg/mL of tantalum, as described previously. Hydrogels were soaked in sterile HUVEC culture medium overnight. Meanwhile, HUVECs were seeded at the density of 30,000 cells/cm^2 in 48-well plates and allowed to attach overnight. The next day, the medium soaked with the hydrogels was pipetted into the cell-laden well plates. Three wells were assigned to each condition. Two plates with the same conditions were made, one to perform the assay on day 1 and the other on day 3.

2.2.11 Live dead assay

To assess the viability of the HUVECs after 1 or 3 days, a Live-Dead dye solution was prepared with a 2 µM calcein AM/4 µM EthD-III concentration in PBS. PBS with 0.05% of Tween and 0.05% of Triton X-100 (PBSTT; 200 µL/well) was added to two wells to make positive controls. Cells cultured in medium only (i.e., no contact with hydrogels) were used as negative controls. Medium was removed from all the wells. To eliminate residual medium, 300 µL/well of PBS was added to the wells, then removed. Live-Dead dye solution was added in each well, incubated 15 minutes at 37°C, and replaced by 300 µL/well of PBS for imaging. Three images of each well at different locations were taken with the 10X objective of a Nikon eclipse TS 100 fluorescence microscope. To assess viability, the number of live and dead cells were determined according to the following definitions:

Number of live cells: number of cells stained with calcein AM. Number of dead cells: number of cells stained with EthD-III.

$$\text{Cell viability} = \frac{\text{number of live cells}}{\text{total number of cells}}$$

2.2.12 Statistical analysis

All data are presented as mean ± S.D. (standard deviation) from at least n=3 experiments. Two-way ANOVA was applied to evaluate the differences between treated and control groups. For all the tests, the level of significance was $p < 0.05$.

2.3 Results

2.3.1 Characterization of PHA

To create an injectable, biodegradable, hyaluronic acid-based material for vascular occlusion of brain blood vessel aneurysms, pentenoate-modified hyaluronic acid (PHA) was first synthesized (Figure 10). The formation of pentenoate groups that characterize PHA was assessed by the presence of hydrogen proton NMR peaks at 6.25 ppm with D_2O solvent (Figure 11). The amount of pentenoate groups was 0.607 mmol of pentenoate per gram of PHA, which confirmed the good quality of the synthetized PHA.

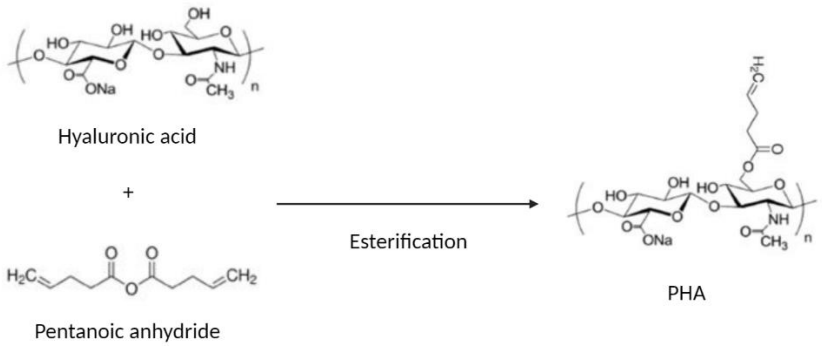


Figure 10: Formation of PHA. Chemical reaction for PHA synthesis. Hyaluronic acid (HA) is combined with pentenoic anhydride under slightly basic conditions (pH 8-9), to obtain pentenoate hyaluronic acid (PHA).

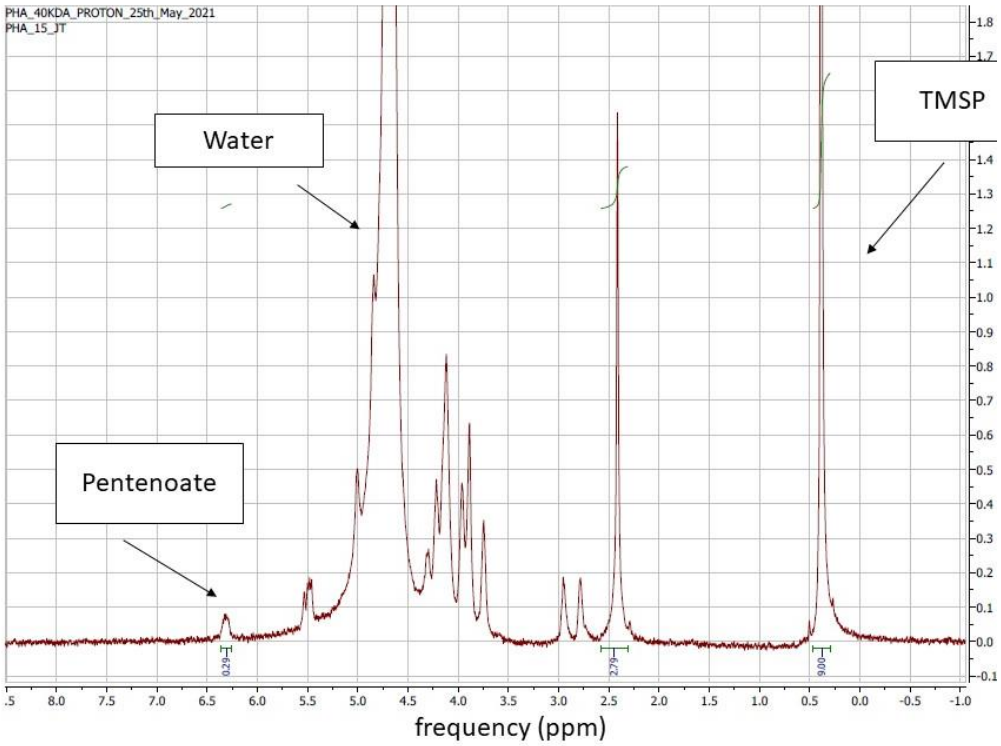


Figure 11: 1H-NMR for PHA Characterization. The peak at 0.25 ppm indicates the presence of TMSP. The peak around 5 ppm indicates the presence of the water. The peak at 6.25 ppm indicates the presence of pentenoate. The ratio of pentenoate mmol per gram of PHA was 0.607 mmol of pentenoate/g of PHA .

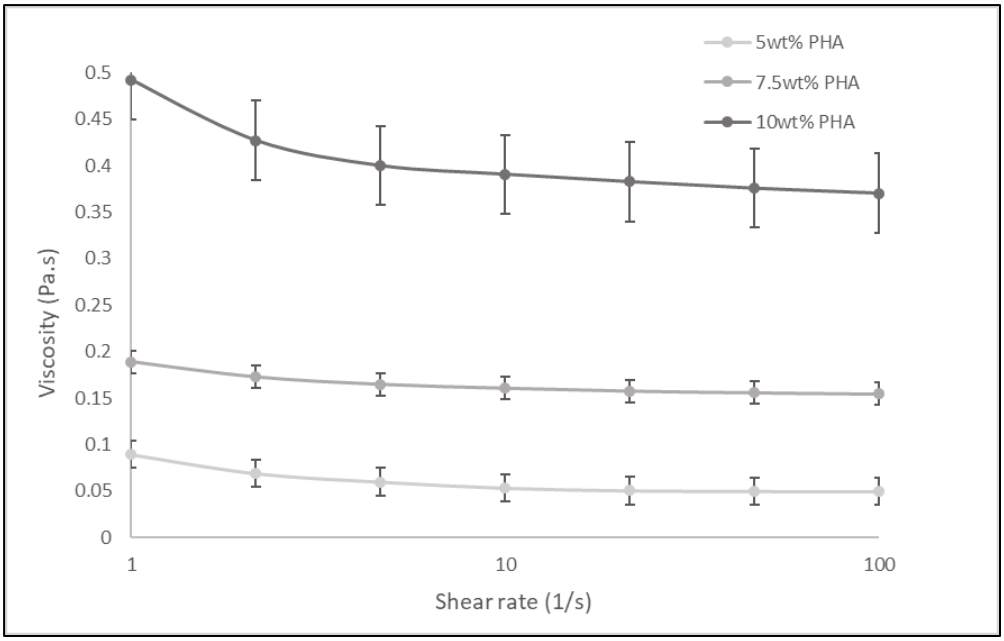
2.3.2 Viscosity of PHA solutions

The liquid solution of PHA/LAP/DTT must have a good flow through a surgical catheter to be delivered to the site of an aneurysm. Viscosity is an indicator of flow which is proportional to it. The viscosity of 5 wt%, 7.5 wt%, and 10 wt% PHA hydrogels increased with increasing weight percent and respectively was, at a shear rate of 10 s^{-1} 0.053 ± 0.015 Pa.s, 0.161 ± 0.012 Pa.s, and 0.391 ± 0.047 Pa.s (Figure 12A).

A

To interpret and support these findings, flow of liquid PHA solution was further assessed by injecting liquid solutions of PHA/LAP/DTT through a surgical catheter of one mm diameter.

A



B

Material	Concentration					
Poly Hyaluronic acid	5 weight %		7.5 weight %		10 weight %	
Tantalum powder	0 mg/mL	50 mg/mL	0 mg/mL	50 mg/mL	0 mg/mL	50 mg/mL
Flowable through 1 mm catheter?	✓	✓	✓	✓	≈	≈

Table 1: Characteristics of our materials regarding capacity to go through a catheter

✓ Flow ≈ No flow

Figure 12: Viscosity and capacity to go through a catheter of our 40 kDa PHA/Tantalum material. (A) The viscosity of 5 wt%, 7.5 wt%, and 10 wt% PHA hydrogels increased with increasing weight percent. (B) With or without tantalum the material could flow through a catheter of 1 mm of diameter when it is composed of 5 wt% and 7.5 wt% of PHA. However, 10 wt% PHA with and without tantalum could not flow through a 1 mm diameter catheter.

Solutions of 5 wt% and 7.5 wt% of PHA with DTT and LAP without and with 50 mg/mL of tantalum powder flowed through the surgical catheter without resistance, whereas solution of 10 wt% of PHA with DTT and LAP could not flow through the catheter, regardless of the presence or absence of tantalum powder (Figure 12B).

2.3.3 X-rays to assess tantalum visibility

During the procedure and once in the patient, surgeons must assess PHA hydrogels correct placement in of aneurysms. Thus, the visibility of tantalum powder within PHA hydrogels was checked with dental X-rays of PHA hydrogels (Figure 13). PHA hydrogels (10 wt%) were formed by combining PHA with LAP and DTT and 0, 5, or 50 mg Ta / mL PHA and exposing them to a 365 nm UV light for 2 minutes (Figure 14). The 10 wt% PHA hydrogels with 50 mg/mL group had more Ta flakes and they were more homogeneously distributed than in the 10 wt% PHA hydrogels with 5 mg of ta per mL of PHA, whereas controls (just PHA) had no tantalum flakes in them. The intensity per mm^2 of tantalum powder increased proportionally with the concentrations of tantalum. The intensity per mm^2 increased from 0.22 to 0.92 between the 10 wt% PHA hydrogels without tantalum and 10 wt% PHA hydrogels with 50 mg of Ta per mL of hydrogel. When ballistic gel and a PLA cover were added to the top of hydrogels, to simulate brain tissues and the skull, respectively, tantalum flakes were still visible in hydrogels. Importantly, the intensity per mm^2 of tantalum powder was not decreased by the presence of the ballistic gels, nor by the PLA cover simulating the skull. The intensity of PHA hydrogels with 50 mg of Ta per mL of PHA was still 0.92 units/mm^2. The quantitative analysis was corroborated by the qualitative observation of X-ray images.

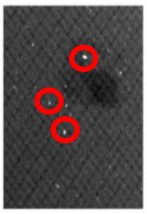
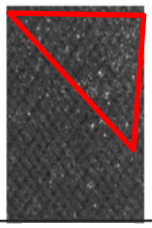
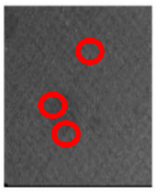
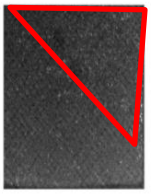
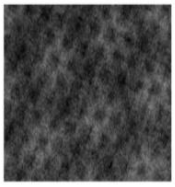
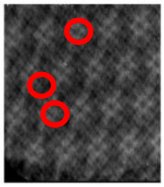
Composition / Cover	PHA	PHA + 5 mg/mL of Tantalum	PHA + 50 mg/mL of Tantalum
Hydrogel only			
Intensity/mm2	0.22	0.36	0.92
hydrogel + Ballistic gel			
Intensity/mm2	0.13	0.22	0.92
hydrogel + ballistic gel + PLA cover			
Intensity/mm2	0.61	0.74	0.92

Figure 13: Tantalum visibility in dental X-rays depending on tantalum concentration and cover on top of PHA. Tantalum flakes are circled and triangled in red. The intensity per mm^2 of tantalum powder increased proportionally with the concentrations of tantalum. The intensity per mm^2 of tantalum powder was not decreased by the presence of 47 mm high ballistic gels simulating brain tissues, not by the 4.8 mm thick PLA covers simulating the skull. The pattern was due to the superposition of ballistic gel and PLA.

2.3.4 Mechanical properties of hydrogels

PHA hydrogels were formed by combining PHA with LAP and DTT and 0 or 50 mg of tantalum per mL of PHA were added. Hydrogels were crosslinked by exposing them to a 365 nm UV light for 2 minutes (Figure 14). Hydrogels of different weight percentages of PHA in PBS were made: 5 wt%, 7.5 wt%, and 10 wt%. All the hydrogels were transparent, 1 mm thick, and had a negligible quantity of bubbles.

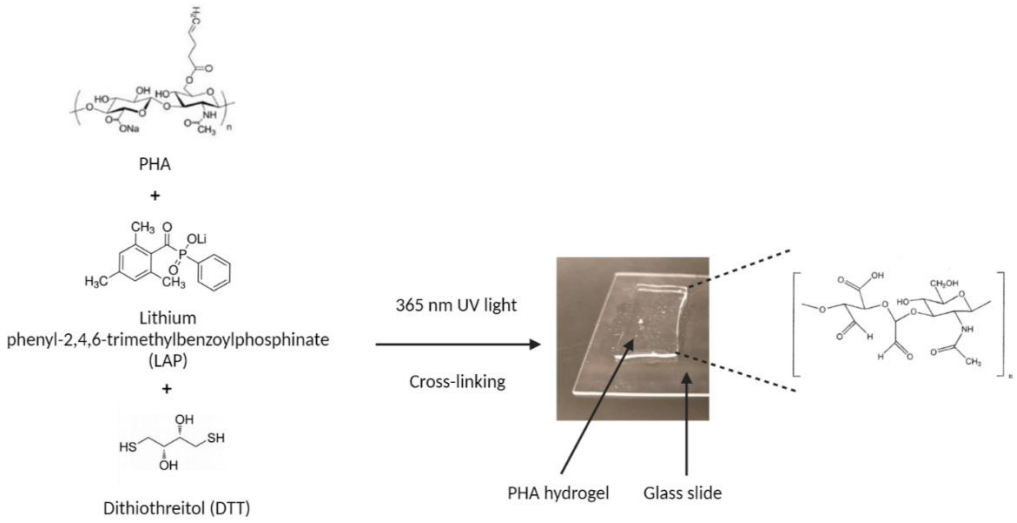


Figure 14: PHA hydrogels formation. To obtain hydrogels, PHA is combined with DTT (cross-linker) and LAP (photo-initiator) under a 365 nm UV light for 2 minutes.

To assess the stiffness of the 5 wt%, 7.5 wt%, and 10 wt% PHA hydrogels and their capacity to reinforce vessels walls, the compressive moduli were characterized by applying a 0.01 N force axially and gradually increasing with a 5 µm/s strain rate until 20% of strain (Figure 15). For hydrogels without tantalum the compression moduli were increased proportionally to hydrogel weight percent. The moduli were respectively 48 ± 15, 68 ± 13, and 97 ± 12 kPa for the 5 wt%, 7.5 wt%,

and 10 wt% PHA hydrogels, where 7.5 wt% and 10 wt% PHA hydrogels had significant differences ($p<0.05$). Similarly, the compression moduli were increasingly proportional to weight percent in the 50 mg/mL tantalum group. The moduli were respectively 42 ± 7, 58 ± 10, and 75 ± 22 kPa for the 5 wt%, 7.5 wt%, and 10 wt% PHA with 50 mg of Ta per mL of PHA groups. There was no significant difference between the tantalum and no tantalum groups.

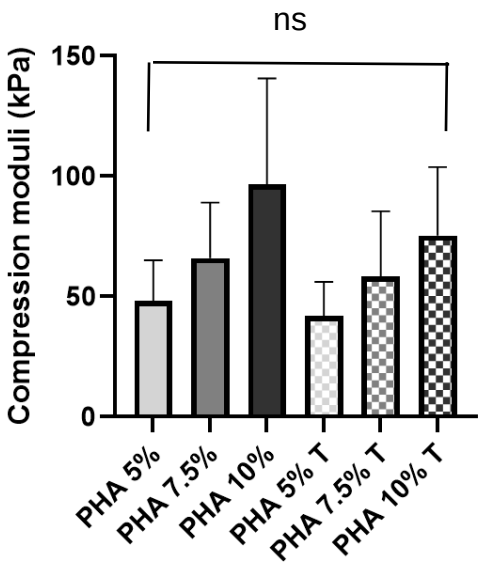


Figure 15: Mechanical characterization of 40 kDa 5 wt%, 7.5 wt%. and 10 wt% PHA hydrogels (n=12) with absence or presence of tantalum powder (50 mg/mL). (P)HA = Pentenoate-modified hyaluronic acid, T = tantalum powder, ns: non-significant. Compression moduli of 5 wt%, 7.5 wt%, and 10 wt% percent weight PHA hydrogels with and without tantalum exhibited increasing moduli with increasing weight percentages.

2.3.5 Swelling Capacity

Swelling capacity is an important parameter to know because it indicates how much the material will swell when it encounters biological fluids and thus, we could adjust the quantity of PHA to deliver in aneurysms. To assess the swelling capacity of 5 wt%, 7.5 wt%, and 10 wt% PHA hydrogels without and with 50 mg of Ta/g of PHA, their water absorption and swelling ratios were measured. Water absorption (swollen weight mg/fabricated weight mg) of 5 wt%, 7.5 wt%. and 10 wt% PHA hydrogels was increasingly proportional to weight percent and 1.7 ± 0.33, 1.9 ± 0.17, and 2.4 ± 0.14, respectively (Figure 16).

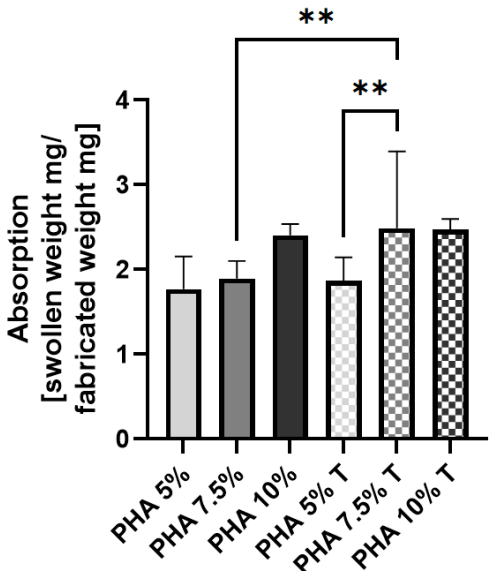


Figure 16: Water absorption of 40 kDa 5 wt%, 7.5 wt%. and 10 wt% PHA hydrogels (n=12) with absence or presence of tantalum powder (50 mg/mL). (P)HA=(Pentenoate) Hyaluronic acid, T= tantalum powder. **: $p < 0.01$. Water absorption ([swollen weight mg/fabricated weight mg]) of 5 wt%, 7.5 wt%, and 10 wt% percent weight PHA hydrogels with and without tantalum exhibited increasing moduli with increasing weight percentages.

Water absorption values for the tantalum groups were respectively 1.9 ± 0.27, 2.5 ± 0.35, and 2.5 ± 0.13 for 5 wt%, 7.5 wt%, and 10 wt% PHA hydrogels with 50 mg of Ta per mL of hydrogel. No significant

difference was observed between the tantalum and no tantalum groups, except for 7.5 wt% hydrogels, where the tantalum group was 1.5 times more absorbent.

The swelling ratio ([swollen weight mg/dry weight mg) of 5 wt%, 7.5 wt%, and 10 wt% PHA hydrogels was inversely proportional to weight percent in the no tantalum group, but not significantly (Figure 17). The ratios were 33 ± 8%, 23 ± 5%, and 20 ± 4% for 5 wt%, 7.5 wt%, and 10 wt% PHA hydrogels. Similarly, the swelling ratio of 5 wt%, 7.5 wt%, and 10 wt% PHA hydrogels with 50 mg of Ta per mL hydrogel, was inversely proportional to weight percent. The ratios were 25 ± 5%, 23 ± 4%, and 23 ± 9% for 5 wt%, 7.5 wt%, and 10 wt% PHA hydrogels.

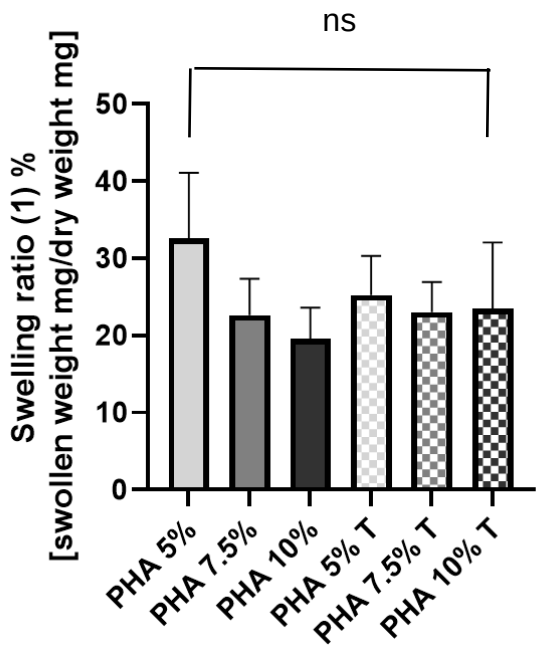


Figure 17: Swelling ratio (swollen weight mg/dry weight mg) of 40 kDa 5 wt%, 7.5 wt%. and 10 wt% PHA hydrogels (n=12) with absence or presence of tantalum powder (50 mg/mL). (P)HA=(Pentenoate) Hyaluronic acid, T= tantalum powder, ns: non-significant.

2.3.6 Cell Viability

To assess the cytocompatibility of PHA hydrogels with human umbilical vein endothelial cells (HUVEC), a calcein AM/EthD-III live dead assay was done (

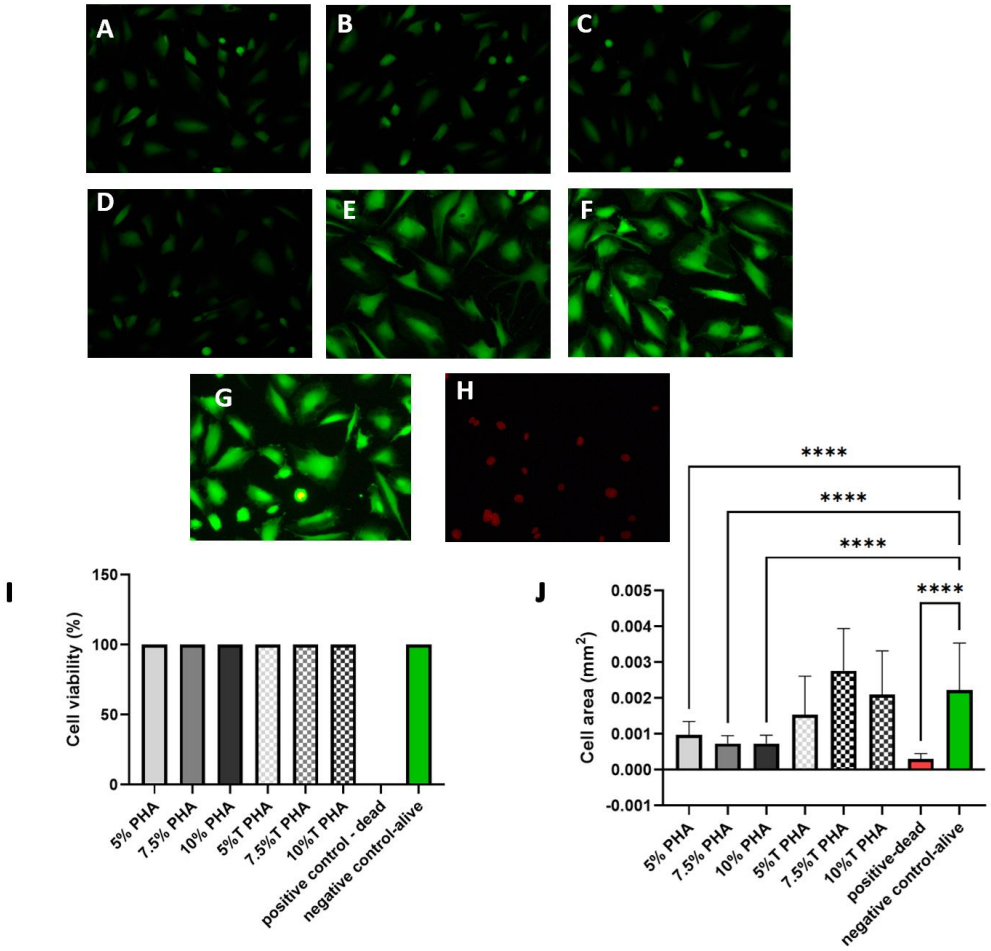


Figure **18**).

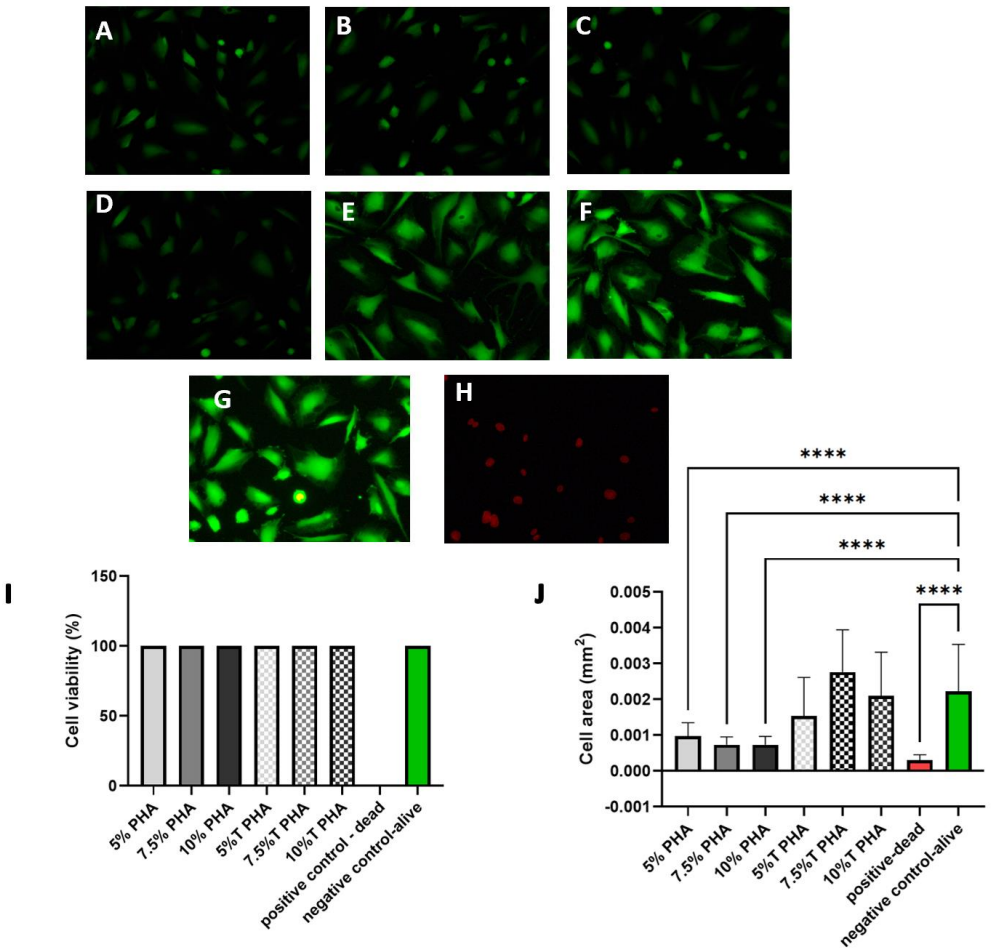


Figure 18: Cell viability of human umbilical vein endothelial cells (HUVEC) after 24 hours in contact with PHA hydrogel-soaked medium. ****: $p < 0.0001$. A to H: Representative images depicting live, dead, and composite images of HUVEC after 24 and 72 hours in contact with HUVEC medium soaked for 24h with (A) 5 wt%, (B) 7.5 wt%, (C) 10 wt%, (D) 5 wt%+50 mg/mL Ta, I 7.5 wt%+50 mg/mL Ta, (F) 10 wt%%+50 mg/mL Ta PHA hydrogels and negative control: (G) no PHA in the medium, (H) positive control: no PHA in medium and cells were killed. Green: calcein AM, red: ethidium homodimer three (EthD-III). Live cells were stained with calcein AM. Dead cells were stained with EthD-III. Graphs representing (I) cell viability (number of live cells/ total number of cells) and (J) cell area (average area in mm^2 of n=21 cells per condition) of HUVEC from the live dead assay. Viability was 100% for all conditions. Cell area of no tantalum group was smaller than the cell area of the tantalum group and smaller than the control.

The cell viability (number of live cells/ total number of cells) of HUVEC from the live dead assay were 100% for all conditions.

2.4 Discussion

Current brain aneurysm treatments, such as surgical clip and coils, allow only partial aneurysm occlusion and partial blood vessel wall reconstruction and these treatments stay in the patient ad vitam, thus having a high risk of vessel wall inflammation[4,25,32]. To address these issues, our approach is catheter-based delivery of an injectable, biodegradable, hyaluronic acid-based material that is compatible with radiographic and magnetic resonance medical imaging techniques, that can be used to plug saccular brain aneurysms and induces vascular regeneration. In these studies, pentanoate hyaluronic acid was synthesized, characterized with proton NMR, and crosslinked into 5, 7.5, and 10% PHA hydrogels. Flow through a 1 mm of diameter catheter of liquid 5 and 7.5% PHA solutions with and without 50 mg of tantalum powder per gram of PHA was laminar, whereas flow of liquid 10% PHA solutions with and without tantalum was turbulent and slow. To enable the visibility of PHA hydrogels in patients, tantalum powder was added inside the hydrogels. X-rays confirmed that 50 mg of tantalum powder per gram of PHA allowed the gels to be seen under PLA and ballistic gels simulating brain tissues and the skull. The compressive elastic moduli of 5 wt%, 7.5 wt%, and 10 wt% PHA hydrogels exhibited increasing moduli with increasing weight percentages and were respectively 48 ± 15, 68 ± 13, and 97 ± 12 kPa for the no tantalum group, and 42 ± 7, 58 ± 10, and 75 ± 22 kPa for the tantalum group. Viability of HUVECs at 24 hours in vascular cell medium infused with 5 wt%, 7.5 wt%, and 10 wt% PHA hydrogels, without and with 50 mg of tantalum powder per gram of PHA, was 100%.

Compressive moduli were measured to evaluate the stiffness of the 5 wt%, 7.5 wt%, and 10 wt% PHA hydrogels and their capacity to reinforce vessels walls. Compressive moduli of 5 wt%, 7.5 wt%, and 10 wt% 40 kDa PHA hydrogels increased proportionally to weight percent, in a range of 50-100 kPa. These results demonstrated that the more crosslinked PHA was, the more resistant to shear stress because more chains of PHA were bound together creating more crosslinked PHA hydrogels[62]. Burdick *et al*.[63] reported that the compressive moduli of 5 and 10% 50 kDa PHA hydrogels were respectively 40 and 75 kPa, which is coherent with our results. Toh *et al.*[64] also found that hyaluronic acid hydrogels of increasing weight percent had increasing compressive moduli, though their range was lower than this present study because their crosslinking degrees were lower. Compressive moduli of 5 wt%, 7.5 wt%, and 10 wt% PHA hydrogels with tantalum also increased proportionally to weight percent in the same range, but for the same weight percent, each modulus in the tantalum group was lower than the one of the no tantalum group, although not significantly. Contrary to our results, Hu *et al.*[65] found that addition of tantalum carbide nanoparticles to poly diacetone acrylamide hydrogels increased their compressive moduli significantly. The difference between studies could be due to the difference of structure and properties of the materials used.

Importantly, our experimental compressive moduli range was similar but slightly superior to brain tissues' compressive moduli. Rashid *et al*.[66] found compressive moduli of brain tissue between 10 and 20 kPa, but they were cutting whole brains and analyzing their compressive

moduli, not testing vessels. The softness of whole brain tissues might decrease the general compressive moduli[66]. Another study found that compressive moduli of blood vessels were between 200 and 600 kPa[67]. These numbers were higher than our results; however, the compressive moduli reported were the average of the whole body, where blood flow speed can be ten times higher than in the brain, which could explain the higher compressive moduli[68,69].

Water absorption was measured to calculate the maximal fluid intake of PHA hydrogels to later include this parameter in our calculations of the quantity of PHA to inject in hydrogels. Water absorption, which was measured as the swollen weight of the hydrogel relative to its fabricated weight, increased with weight percent in 5, 7.5, and 10% PHA hydrogels. The same trend was observed for 5, 7.5, and 10% PHA hydrogels with tantalum and the results had the same order of magnitude. These findings correlate with the fact that the more crosslinked hydrogels are, the more it structure has pores in which water can be stored[64]. These results allow for the determination how much fluid can be absorbed by PHA hydrogel. As PHA is expected to behave the same way in blood because PBS and blood have similar pH and main ionic constituants[70], PBS was utilized to determine water absorbance in these studies. For instance, PHA 10% have an absorption rate of 2.5. Thus, when delivering the PHA hydrogel, it is expected that the quantity of 10% PHA to inject in a patient's aneurism must be diminished by 2.5 times to prevent overpopulating the aneurysm site with material.

Similarly to water absorption, swelling ratio was measured to evaluate the total fluid intake of PHA between its swollen and dry forms. The swelling ratio, which was calculated from the swollen weight of the hydrogel minus the dry weight of the hydrogel divided by the dry weight, of 5%, 7.5%, and 10% percent weight PHA hydrogels without tantalum, exhibited decreasing moduli with increasing weight percentages. These results were expected because this ratio includes dry PHA which doesn't have water and indicates that more PHA is crosslinked, the more its organized structure allows water to be withdrawn from it, but also the more it can re-absorb water. Burdick *et al*.[63], reported that the swelling ratio of 5, 10 and 20% 50 kDa PHA hydrogels were decreasing with increasing weight percentages. The swelling ratio of 5 wt% compared to the 7.5 wt%, and the 5 wt% compared to the 10 wt% PHA hydrogels with 50 mg of tantalum per mL of PHA, were also decreasing with increasing crosslinking rate, which is coherent to the results of the no tantalum group. The swelling ratio helps to determine how much PHA hydrogels swell from their dry form to calculate the amount PHA that needs to be made for storage and shipping.

The liquid solution of PHA/LAP/DTT must have a good flow through a surgical catheter to be delivered to the site of an aneurysm, flow that is indicated by PHA hydrogels viscosity. The viscosity of 5 wt%, 7.5 wt%, and 10 wt% PHA hydrogels increased with increasing weight percent and respectively was shear rate of 10 s^{-1} 00.053 ± 0.015 Pa.s, 0.161 ± 0.012 Pa.s, and 0.391 ± 0.047. Kiyotake *et al.*[61] found a similar viscosity of 8 Pa.s at a shear rate of 10 s^{-1} for 4 wt% PHA hydrogels. Kim

et al.[71] found that viscosity of HA hydrogels increased with increasing weight percent. Viscosity results correlated with the fact that 5 wt% and 7.5 wt% PHA hydrogel solutions could flow easily through a 1 mm of diameter catheter, whereas 10 wt% PHA hydrogel solutions were more difficult to deliver through the catheter. As such, we believe that 5 wt% and 7.5 wt% PHA liquid hydrogels could be easily delivered into aneurysm sites and crosslinked in place. However, delivery of 10 wt% PHA solutions may prove more challenging and would likely need chemicals that modify its viscosity to be useful in clinic.

Correct placement of PHA hydrogels in aneurysms was assessed with dental X-rays of PHA hydrogels. Our x-ray images of 10 wt% PHA hydrogels with 5 or 50 mg Ta/mL showed that tantalum flakes are visible in x-rays pictures of these hydrogels, whereas PHA hydrogels without tantalum could not be differentiated from the background. However, when 10 wt% PHA hydrogels with 5 mg Ta/mL are covered with ballistic gels and PLA to simulate brain tissues and the skull[72], tantalum flakes are barely visible, whereas tantalum flakes are visible in 10 wt% PHA hydrogels with 50 mg Ta/mL. The comparison of the intensity per mm^2 of tantalum flakes showed that the intensity of tantalum flakes in the 50 mg/mL group was 2.5 greater compared to the intensity of the Ta flakes in the 5 mg/mL group. Other studies used 138 mg/mL to 240 mg/mL of tantalum to image rat and rabbit blood vessels; however, in these studies, tantalum was directly injected into the bloodstream, which diluted the material by a factor ten. Thus, the actual tantalum concentrations in blood were between 14 and 25 mg/mL, which is the

same order of magnitude than ours[56–59]. It means that our material must be seen *in vivo* through the skull and brain tissues. Thus, we could monitor the injection non-invasively and provide follow-up to determine whether the treatment was working.

PHA hydrogels need to be compatible with HUVEC because blood vessels are coated with these cells. Our results demonstrate that HUVECs in contact for 24 hours with cell medium infused with our material had a survival rate of a 100%. It means that our material does not induce cell death *in vitro*. Kim *et al.*[73] put mesenchymal stem cells in HA hydrogels and reported a viability of 72% after two days. Kang *et al*.[74] showed that osteoblasts treated with 10 µg/mL of tantalum nanoparticles had a 20% increased viability, compared to non-treated osteoblasts. Measures of cell area showed that average areas of 5 wt%, 7.5 wt%, and 10 wt% PHA hydrogels without tantalum have cell areas that are at least two times smaller than cells treated with controls only. However, the areas of HUVECs treated with PHA hydrogels containing tantalum were similar to the areas of cells exposed to medium only. These results might mean that the presence of PHA reduces cell area, but cells area may also be smaller because the cells are dividing. Balla *et al.*[75] studied the morphology of human fetal osteoblasts cultivated on porous tantalum, and found that cells had a traditional shape, were spread, and formed cellular micro-extensions as filopodia.

Chapter 3: Conclusions and recommendations

3.1 Conclusions

Brain aneurysms are deformations of brain blood vessel walls. In the United States, one out of 50 people have at least one unruptured aneurysm, with up to 50% of rupture hazard depending on the location of the aneurysm[1,2]. Aneurysm rupture causes brain hemorrhages that are lethal for half of the patients or lead to brain function losses for two third of the surviving patients[2]. Current treatments as surgical clip and coils allow partial aneurysm occlusion and partial blood vessel wall reconstruction and these treatments stay in the patient ad vitam, thus having a high risk of vessel wall inflammation[4,25,32]. To address these issues, our approach is catheter-based delivery of an injectable, hyaluronic acid-based material that is compatible with radiographic and magnetic resonance medical imaging techniques. This material can be used to plug saccular brain aneurysms and induce vascular regeneration. To assess whether PHA hydrogel matches the compressive resistance of vessel walls, compressive moduli of 5, 7.5, and 10% PHA hydrogels without or with 50 mg of Ta per g of PHA were measured. The compressive moduli of 5, 7.5, and 10% PHA hydrogels without or with 50 mg of Ta per g of PHA increased with weight percent and were comprised within a 50 to 100 kPa range, which is the range of brain tissues' compressive moduli. There was no significant difference between the compressive moduli of PHA hydrogels with or without tantalum powder. To verify the biocompatibility of PHA hydrogels with blood vessels, the cell viability of human umbilical vein endothelial cells

(HUVEC) in contact with medium infused for 24 hours with 5, 7.5, and 10% PHA hydrogels without or with 50 mg of Ta per g of PHA was quantified. The viability of HUVEC exposed to 5, 7.5, and 10% PHA hydrogels without or with 50 mg of Ta per g of PHA was a 100%. These data point out that injectable 5 and 7.5% PHA hydrogels with compressive moduli like brain tissues and good viability with endothelial cells can be made to potentially plug brain aneurysms.

To conclude, we proposed a possible brain aneurysm treatment that can be injected in brain aneurysms via a microcatheter without opening patients' skulls, can be imaged with X-rays to ensure correct placement, has a compressive resistance close to blood vessels' resistance, and has a high cell viability.

3.2 Recommendations

This study has shown promising results for the treatment of brain aneurysms with a minimally invasive method that promotes cell regeneration. However, further research is required to validate some results and test the treatment *in vivo*.

First, the assessment of HUVEC proliferation by comparing cell growth over time would highlight PHA's impact on cell growth and our treatment's capacity to enhance cell regeneration. To earn more information on cell regeneration, a scratch assay can be done. It consists in cultivating cells in contact with PHA infused medium, scratching the cells to form a line, and observing how fast the line is filled with cells compared to the same experiment with cells that were not in contact with

PHA. The expected results would be to see that PHA hydrogels enhance cell proliferation.

Furthermore, the evaluation of PHA hydrogels degradation would confirm that PHA disappear progressively, along with the disappearance of the aneurysm and the reformation of the blood vessel well. To test this property, it could be interesting to crosslink PHA in an aneurysm model and then expose it to a constant flow of water with the speed of blood flow in one of the main cerebral arteries and monitor the degradation time of PHA.

Finally, it is necessary to test this treatment in an aneurysm model, either in vivo if all the required authorizations are obtained, or in a 3D bio-printed model. In the literature, most animals used to make aneurysm models were rabbits[76,77], rats[78,79], and pigs[80–82]. Regardless of the animal used, the aneurysms were induced by infusion with elastase which concentration and origin varied depending on the model[76,78,79], or mechanically induced by cutting an artery and inserting a clamp or a patch of another organ to form the aneurysm sac[77,82] , or by combining both techniques[80,81]. In such models, delivery of PHA and crosslinking could be tested. Then, cytotoxicity and cell regeneration could be evaluated, and PHA and aneurysm degradations could be monitored.

References

(1) Abecassis, I. J.; Zeeshan, Q.; Ghodke, B. V.; Levitt, M. R.; Ellenbogen, R. G.; Sekhar, L. N. Surgical Versus Endovascular Management of Ruptured and Unruptured Intracranial Aneurysms: Emergent Issues and Future Directions. *World Neurosurgery* **2020**, *136*, 17–27. https://doi.org/10.1016/j.wneu.2019.12.127.

(2) Statistics and Facts. *Brain Aneurysm Foundation*.

(3) Brinjikji, W.; Kallmes, D. F.; Lanzino, G.; Cloft, H. J. Hospitalization Costs for Endovascular and Surgical Treatment of Unruptured Cerebral Aneurysms in the United States Are Substantially Higher than Medicare Payments. *AJNR Am J Neuroradiol* **2012**, *33* (1), 49–51. https://doi.org/10.3174/ajnr.A2739.

(4) Molyneux, A. J.; Birks, J.; Clarke, A.; Sneade, M.; Kerr, R. S. C. The Durability of Endovascular Coiling versus Neurosurgical Clipping of Ruptured Cerebral Aneurysms: 18 Year Follow-up of the UK Cohort of the International Subarachnoid Aneurysm Trial (ISAT). *Lancet* **2015**, *385* (9969), 691–697. https://doi.org/10.1016/S0140-6736(14)60975-2.

(5) Tucker, W. D.; Arora, Y.; Mahajan, K. Anatomy, Blood Vessels. In *StatPearls*; StatPearls Publishing: Treasure Island (FL), 2021.

(6) *Classification & Structure of Blood Vessels | SEER Training*. https://training.seer.cancer.gov/anatomy/cardiovascular/blood/classification.html (accessed 2021-05-21).

(7) Etminan, N.; Rinkel, G. J. Unruptured Intracranial Aneurysms: Development, Rupture and Preventive Management. *Nat Rev Neurol* **2016**, *12* (12), 699–713. https://doi.org/10.1038/nrneurol.2016.150.

(8) Xu, J.; Shi, G.-P. Vascular Wall Extracellular Matrix Proteins and Vascular Diseases. *Biochim Biophys Acta* **2014**, *1842* (11), 2106–2119. https://doi.org/10.1016/j.bbadis.2014.07.008.

(9) Kapellos, G. E.; Alexiou, T. S. Chapter 1 - Modeling Momentum and Mass Transport in Cellular Biological Media: From the Molecular to the Tissue Scale. In *Transport in Biological Media*; Becker, S. M., Kuznetsov, A. V., Eds.; Elsevier: Boston, 2013; pp 1–40. https://doi.org/10.1016/B978-0-12-415824-5.00001-1.

(10) Pillinger, N. L.; Kam, P. C. A. Endothelial Glycocalyx: Basic Science and Clinical Implications. *Anaesth Intensive Care* **2017**, *45* (3), 295–307. https://doi.org/10.1177/0310057X1704500305.

(11) Milutinović, A.; Šuput, D.; Zorc-Pleskovič, R. Pathogenesis of Atherosclerosis in the Tunica Intima, Media, and Adventitia of Coronary Arteries: An Updated Review. *Bosn J Basic Med Sci* **2020**, *20* (1), 21–30. https://doi.org/10.17305/bjbms.2019.4320.

(12) Sadowitz, B.; Seymour, K.; Gahtan, V.; Maier, K. G. The Role of Hyaluronic Acid in Atherosclerosis and Intimal Hyperplasia. *Journal of Surgical Research* **2012**, *173* (2), e63–e72. https://doi.org/10.1016/j.jss.2011.09.025.

(13) Etminan, N.; Dreier, R.; Buchholz, B. A.; Beseoglu, K.; Bruckner, P.; Matzenauer, C.; Torner, J. C.; Brown, R. D.; Steiger, H.-J.;

Hänggi, D.; Macdonald, R. L. Age of Collagen in Intracranial Saccular Aneurysms. *Stroke* **2014**, *45* (6), 1757–1763. https://doi.org/10.1161/STROKEAHA.114.005461.
(14) Dong, H.; Blaivas, M.; Wang, M. M. Bidirectional Encroachment of Collagen into the Tunica Media in Cerebral Autosomal Dominant Arteriopathy with Subcortical Infarcts and Leukoencephalopathy. *Brain Research* **2012**, *1456*, 64–71. https://doi.org/10.1016/j.brainres.2012.03.037.
(15) Suh, C.-M.; Kim, S.-H.; Monson, K. L.; Goldsmith, W. Tensile Characteristics and Behavior of Blood Vessels from Human Brain in Uniaxial Tensile Test. *KSME International Journal* **2003**, *17* (7), 1016–1025. https://doi.org/10.1007/BF02982986.
(16) Monson, K. L.; Goldsmith, W.; Barbaro, N. M.; Manley, G. T. Axial Mechanical Properties of Fresh Human Cerebral Blood Vessels. *Journal of Biomechanical Engineering* **2003**, *125* (2), 288–294. https://doi.org/10.1115/1.1554412.
(17) Camasão, D. B.; Mantovani, D. The Mechanical Characterization of Blood Vessels and Their Substitutes in the Continuous Quest for Physiological-Relevant Performances. A Critical Review. *Materials Today Bio* **2021**, *10*, 100106. https://doi.org/10.1016/j.mtbio.2021.100106.
(18) Kulcsár, Z.; Ugron, Á.; Marosfői, M.; Berentei, Z.; Paál, G.; Szikora, I. Hemodynamics of Cerebral Aneurysm Initiation: The Role of Wall Shear Stress and Spatial Wall Shear Stress Gradient. *American Journal of Neuroradiology* **2011**, *32* (3), 587–594. https://doi.org/10.3174/ajnr.A2339.
(19) Xiao, W.; Qi, T.; He, S.; Li, Z.; Ou, S.; Zhang, G.; Liu, X.; Huang, Z.; Liang, F. Low Wall Shear Stress Is Associated with Local Aneurysm Wall Enhancement on High-Resolution MR Vessel Wall Imaging. *American Journal of Neuroradiology* **2018**, *39* (11), 2082–2087. https://doi.org/10.3174/ajnr.A5806.
(20) Frösen, J.; Cebral, J.; Robertson, A. M.; Aoki, T. Flow-Induced, Inflammation-Mediated Arterial Wall Remodeling in the Formation and Progression of Intracranial Aneurysms. *Neurosurgical Focus* **2019**, *47* (1), E21. https://doi.org/10.3171/2019.5.FOCUS19234.
(21) Chalouhi, N.; Hoh, B. L.; Hasan, D. Review of Cerebral Aneurysm Formation, Growth, and Rupture. *Stroke* **2013**, *44* (12), 3613–3622. https://doi.org/10.1161/STROKEAHA.113.002390.
(22) Wang, F.; Xu, B.; Sun, Z.; Wu, C.; Zhang, X. Wall Shear Stress in Intracranial Aneurysms and Adjacent Arteries. *Neural Regen Res* **2013**, *8* (11), 1007–1015. https://doi.org/10.3969/j.issn.1673-5374.2013.11.006.
(23) Boussel, L.; Rayz, V.; McCulloch, C.; Martin, A.; Acevedo-Bolton, G.; Lawton, M.; Higashida, R.; Smith, W. S.; Young, W. L.; Saloner, D. Aneurysm Growth Occurs at Region of Low Wall Shear Stress. *Stroke* **2008**, *39* (11), 2997–3002. https://doi.org/10.1161/STROKEAHA.108.521617.
(24) Hanel, R. A.; Cortez, G. M.; Benalia, V. H. C.; Sheffels, E.; Sutphin, D. J.; Pederson, J. M.; Pereira, V. M. Patient Outcomes

after Treatment of Brain Aneurysm in Small Diameter Vessels with the Silk Vista Baby Flow Diverter: A Systematic Review: *Interventional Neuroradiology* **2022**. https://doi.org/10.1177/15910199221091645.
(25) Zhao, J.; Lin, H.; Summers, R.; Yang, M.; Cousins, B. G.; Tsui, J. Current Treatment Strategies for Intracranial Aneurysms: An Overview. *Angiology* **2018**, *69* (1), 17–30. https://doi.org/10.1177/0003319717700503.
(26) *Angiogenesis Inhibitors - National Cancer Institute*. https://www.cancer.gov/about-cancer/treatment/types/immunotherapy/angiogenesis-inhibitors-fact-sheet (accessed 2021-06-22).
(27) Raper, D. M. S.; Rutledge, C.; Winkler, E. A.; Abla, A. A. Definitive Treatment With Microsurgical Clipping After Recurrence and Rerupture of Coiled Anterior Cerebral Artery Aneurysms. *Oper Neurosurg (Hagerstown)* **2020**, *19* (4), 393–402. https://doi.org/10.1093/ons/opaa103.
(28) Engele, T.; Brettschneider, C.; Emami, P.; König, H.-H. Cost Comparison of Surgical Clipping and Endovascular Coiling of Unruptured Intracranial Aneurysms: A Systematic Review. *World Neurosurgery* **2019**, *125*, 461–468. https://doi.org/10.1016/j.wneu.2019.01.195.
(29) Surgical Treatment: Clipping. *Brain Aneurysm Foundation*.
(30) Hoffman, H.; Jalal, M. S.; Chin, L. S. A Propensity Score-Matched Comparison of Readmission Rates Associated With Microsurgical Clipping and Endovascular Treatment of Ruptured Intracranial Aneurysms. *Journal of Stroke and Cerebrovascular Diseases* **2020**, *29* (5), 104696. https://doi.org/10.1016/j.jstrokecerebrovasdis.2020.104696.
(31) Medtronic. *Aneurysm Flow Diversion - About the Therapy*. https://www.medtronic.com/us-en/patients/treatments-therapies/aneurysm-flow-diversion/about.html (accessed 2021-05-25).
(32) Schob, S.; Hoffmann, K.-T.; Richter, C.; Bhogal, P.; Köhlert, K.; Planitzer, U.; Ziganshyna, S.; Lindner, D.; Scherlach, C.; Nestler, U.; Meixensberger, J.; Quäschling, U. Flow Diversion beyond the Circle of Willis: Endovascular Aneurysm Treatment in Peripheral Cerebral Arteries Employing a Novel Low-Profile Flow Diverting Stent. *Journal of NeuroInterventional Surgery* **2019**, *11* (12), 1227–1234. https://doi.org/10.1136/neurintsurg-2019-014840.
(33) Fiorella, D.; Boulos, A.; Turk, A. S.; Siddiqui, A. H.; Arthur, A. S.; Diaz, O.; Lopes, D. K. The Safety and Effectiveness of the LVIS Stent System for the Treatment of Wide-Necked Cerebral Aneurysms: Final Results of the Pivotal US LVIS Trial. *Journal of NeuroInterventional Surgery* **2019**, *11* (4), 357–361. https://doi.org/10.1136/neurintsurg-2018-014309.
(34) Hong, B.; Patel, N. V.; Gounis, M. J.; DeLeo, M. J., III; Linfante, I.; Wojak, J. C.; Wakhloo, A. K. SEMI-JAILING TECHNIQUE FOR COIL EMBOLIZATION OF COMPLEX, WIDE-NECKED INTRACRANIAL ANEURYSMS. *Neurosurgery* **2009**, *65* (6),

1131–1139. https://doi.org/10.1227/01.NEU.0000356983.23189.16.
(35) Jankowitz, B. T.; Thomas, A.; Jovin, T.; Horowitz, M. Y Stenting Using Kissing Stents for the Treatment of Bifurcation Aneurysms. *Journal of NeuroInterventional Surgery* **2012**, *4* (1), 16–21. https://doi.org/10.1136/jnis.2010.004275.
(36) Padalino, D. J.; Singla, A.; Jacobsen, W.; Deshaies, E. M. Enterprise Stent for Waffle-Cone Stent-Assisted Coil Embolization of Large Wide-Necked Arterial Bifurcation Aneurysms. *Surg Neurol Int* **2013**, *4*, 9. https://doi.org/10.4103/2152-7806.106268.
(37) *PK Papyrus*. https://pkpapyrus.com/brochure/ (accessed 2021-11-16).
(38) Health, C. for D. and R. COVERA™ Vascular Covered Stent - P170042/S002. *FDA* **2019**.
(39) Purves, D.; Augustine, G. J.; Fitzpatrick, D.; Katz, L. C.; LaMantia, A.-S.; McNamara, J. O.; Williams, S. M. The Blood Supply of the Brain and Spinal Cord. *Neuroscience. 2nd edition* **2001**.
(40) Fries, F. Neue Wege zur Embolisation von Aneurysmen (Flüssigembolisat). *Radiologe* **2020**, *60* (4), 325–328. https://doi.org/10.1007/s00117-020-00668-4.
(41) Medtronic. *Peripheral Embolization Products - Onyx Liquid Embolic System*. https://europe.medtronic.com/xd-en/healthcare-professionals/products/cardiovascular/peripheral-embolization/onyx.html (accessed 2021-05-25).
(42) Chalouhi, N.; Tjoumakaris, S.; Gonzalez, L. F.; Hasan, D.; Alkhalili, K.; Dumont, A. S.; Rosenwasser, R.; Jabbour, P. Endovascular Treatment of Distal Intracranial Aneurysms with Onyx 18/34. *Clinical Neurology and Neurosurgery* **2013**, *115* (12), 2528–2532. https://doi.org/10.1016/j.clineuro.2013.10.018.
(43) Szikora, I.; Seifert, P.; Hanzely, Z.; Kulcsar, Z.; Berentei, Z.; Marosfoi, M.; Czirjak, S.; Vajda, J.; Nyary, I. Histopathologic Evaluation of Aneurysms Treated with Guglielmi Detachable Coils or Matrix Detachable Microcoils. *AJNR Am J Neuroradiol* **2006**, *27* (2), 283–288.
(44) You, H.; Lee, E.-U.; Kim, Y.-K.; Kim, B.-C.; Park, J.-Y.; Lim, H.-C.; Lee, J.-S.; Noh, I.; Jung, U.-W.; Choi, S.-H. Biocompatibility and Resorption Pattern of Newly Developed Hyaluronic Acid Hydrogel Reinforced Three-Layer Poly (Lactide-Co-Glycolide) Membrane: Histologic Observation in Rabbit Calvarial Defect Model. *Biomater Res* **2014**, *18* (1), 12. https://doi.org/10.1186/2055-7124-18-12.
(45) Hertegård, S.; Nagubothu, S. R.; Malmström, E.; Ström, C. E.; Tolf, A.; Davies, L. C.; Le Blanc, K. Hyaluronan Hydrogels for the Local Delivery of Mesenchymal Stromal Cells to the Injured Vocal Fold. *Stem Cells and Development* **2019**, *28* (17), 1177–1190. https://doi.org/10.1089/scd.2019.0102.
(46) *Injectable in situ cross-linking chitosan-hyaluronic acid based hydrogels for abdominal tissue regeneration | Scientific Reports*.

https://www.nature.com/articles/s41598-017-02962-z (accessed 2022-03-02).
(47) Hong, L.; Shen, M.; Fang, J.; Wang, Y.; Bao, Z.; Bu, S.; Zhu, Y. Hyaluronic Acid (HA)-Based Hydrogels for Full-Thickness Wound Repairing and Skin Regeneration. *J Mater Sci: Mater Med* **2018**, *29* (9), 150. https://doi.org/10.1007/s10856-018-6158-x.
(48) Ghose, S.; Biswas, S.; Datta, K.; Tyagi, R. K. Dynamic Hyaluronan Drives Liver Endothelial Cells towards Angiogenesis. *BMC Cancer* **2018**, *18* (1), 648. https://doi.org/10.1186/s12885-018-4532-1.
(49) *Photoinitiated polymerization of PEG-diacrylate with lithium phenyl-2,4,6-trimethylbenzoylphosphinate: polymerization rate and cytocompatibility - ScienceDirect*. https://www.sciencedirect.com/science/article/pii/S0142961209009041?casa_token=0P561E9gARoAAAAA:bKPfeYqOkTUjfiMpTti7rSqaC6XEwvdCHTwTr8W1cviT_LctOS2ZREayHMYPdRt43byPWg5s-ao (accessed 2021-06-04).
(50) Nguyen, A. K.; Goering, P. L.; Reipa, V.; Narayan, R. J. Toxicity and Photosensitizing Assessment of Gelatin Methacryloyl-Based Hydrogels Photoinitiated with Lithium Phenyl-2,4,6-Trimethylbenzoylphosphinate in Human Primary Renal Proximal Tubule Epithelial Cells. *Biointerphases* **2019**, *14* (2), 021007. https://doi.org/10.1116/1.5095886.
(51) McCall, J. D.; Anseth, K. S. Thiol–Ene Photopolymerizations Provide a Facile Method To Encapsulate Proteins and Maintain Their Bioactivity. *Biomacromolecules* **2012**, *13* (8), 2410–2417. https://doi.org/10.1021/bm300671s.
(52) *Sudden, severe headache: an unexpected culprit - The Lancet*. https://www.thelancet.com/journals/lancet/article/PIIS0140-6736%2814%2960083-0/fulltext (accessed 2021-11-19).
(53) Health, C. for D. and R. Fluoroscopy. *FDA* **2021**.
(54) Fu, J.; Guo, J.; Qin, A.; Yu, X.; Zhang, Q.; Lei, X.; Huang, Y.; Chen, M.; Li, J.; Zhang, Y.; Liu, J.; Dang, Y.; Wu, D.; Zhao, X.; Lin, Z.; Lin, Y.; Li, S.; Zhang, L. Bismuth Chelate as a Contrast Agent for X-Ray Computed Tomography. *J Nanobiotechnology* **2020**, *18*. https://doi.org/10.1186/s12951-020-00669-4.
(55) Koç, M. M.; Aslan, N.; Kao, A. P.; Barber, A. H. Evaluation of X-Ray Tomography Contrast Agents: A Review of Production, Protocols, and Biological Applications. *Microscopy Research and Technique* **2019**, *82* (6), 812–848. https://doi.org/10.1002/jemt.23225.
(56) Roberts, J.; Bonitatibus, P.; Butts, M.; Colborn, R.; Edic, P.; Fitzgerald, P.; Lambert, J.; Marino, M.; Torres, A.; Yeh, B. *Physiochemical, Biological, and Imaging Performance of Zwitterionic-Coated TaO Nanoparticles as CT Contrast Agents*; 2015. https://doi.org/10.13140/RG.2.1.3352.3687.
(57) Rathnayake, S.; Mongan, J.; Torres, A. S.; Colborn, R.; Gao, D.-W.; Yeh, B. M.; Fu, Y. In Vivo Comparison of Tantalum, Tungsten, and Bismuth Enteric Contrast Agents to Complement Intravenous Iodine for Double-Contrast Dual-Energy CT of the

Bowel. *Contrast Media Mol Imaging* **2016**, *11* (4), 254–261. https://doi.org/10.1002/cmmi.1687.
(58) FitzGerald, P. F.; Butts, M. D.; Roberts, J. C.; Colborn, R. E.; Torres, A. S.; Lee, B. D.; Yeh, B. M.; Bonitatibus, P. J. A Proposed CT Contrast Agent Using Carboxybetaine Zwitterionic Tantalum Oxide Nanoparticles: Imaging, Biological, and Physicochemical Performance. *Invest Radiol* **2016**, *51* (12), 786–796. https://doi.org/10.1097/RLI.0000000000000279.
(59) Tantalum Oxide Nanoparticles as Imaging Agents for X-Ray/ Computed Tomography and Methods for Making Same, January 25, 2008.
(60) Wang, Q.; Zhang, H.; Li, Q.; Ye, L.; Gan, H.; Liu, Y.; Wang, H.; Wang, Z. Biocompatibility and Osteogenic Properties of Porous Tantalum. *Experimental and Therapeutic Medicine* **2015**, *9* (3), 780–786. https://doi.org/10.3892/etm.2015.2208.
(61) *Conductive and injectable hyaluronic acid/gelatin/gold nanorod hydrogels for enhanced surgical translation and bioprinting - Kiyotake - 2022 - Journal of Biomedical Materials Research Part A - Wiley Online Library*. https://onlinelibrary.wiley.com/doi/abs/10.1002/jbm.a.37294 (accessed 2022-02-16).
(62) Chimene, D.; Kaunas, R.; Gaharwar, A. K. Hydrogel Bioink Reinforcement for Additive Manufacturing: A Focused Review of Emerging Strategies. *Advanced Materials* **2020**, *32* (1), 1902026. https://doi.org/10.1002/adma.201902026.
(63) Burdick, J. A.; Chung, C.; Jia, X.; Randolph, M. A.; Langer, R. Controlled Degradation and Mechanical Behavior of Photopolymerized Hyaluronic Acid Networks. *Biomacromolecules* **2005**, *6* (1), 386–391. https://doi.org/10.1021/bm049508a.
(64) Toh, W. S.; Lim, T. C.; Kurisawa, M.; Spector, M. Modulation of Mesenchymal Stem Cell Chondrogenesis in a Tunable Hyaluronic Acid Hydrogel Microenvironment. *Biomaterials* **2012**, *33* (15), 3835–3845. https://doi.org/10.1016/j.biomaterials.2012.01.065.
(65) Hu, X.; Wang, Y.; Xu, M. Study of the Cell Responses in Tantalum Carbide Nanoparticles-Enriched Polysaccharide Composite Hydrogel. *International Journal of Biological Macromolecules* **2019**, *135*, 501–511. https://doi.org/10.1016/j.ijbiomac.2019.05.191.
(66) Rashid, B.; Destrade, M.; Gilchrist, M. D. Mechanical Characterization of Brain Tissue in Compression at Dynamic Strain Rates. *Journal of the Mechanical Behavior of Biomedical Materials* **2012**, *10*, 23–38. https://doi.org/10.1016/j.jmbbm.2012.01.022.
(67) Ebrahimi, A. P. Mechanical Properties of Normal and Diseased Cerebrovascular System. *J Vasc Interv Neurol* **2009**, *2* (2), 155–162.
(68) Zarrinkoob, L.; Ambarki, K.; Wåhlin, A.; Birgander, R.; Eklund, A.; Malm, J. Blood Flow Distribution in Cerebral Arteries. *J Cereb*

Blood Flow Metab **2015**, *35* (4), 648–654. https://doi.org/10.1038/jcbfm.2014.241.
(69) Lotz, J.; Meier, C.; Leppert, A.; Galanski, M. Cardiovascular Flow Measurement with Phase-Contrast MR Imaging: Basic Facts and Implementation. *RadioGraphics* **2002**, *22* (3), 651–671. https://doi.org/10.1148/radiographics.22.3.g02ma11651.
(70) Bhandare, P.; Mendelson, Y.; Stohr, E.; Peura, R. A. Glucose Determination in Simulated Blood Serum Solutions by Fourier Transform Infrared Spectroscopy: Investigation of Spectral Interferences. *Vibrational Spectroscopy* **1994**, *6* (3), 363–378. https://doi.org/10.1016/0924-2031(93)E0059-B.
(71) Kim, J.; Chang, J.-Y.; Kim, Y.-Y.; Kim, M.-J.; Kho, H.-S. Effects of Molecular Weight of Hyaluronic Acid on Its Viscosity and Enzymatic Activities of Lysozyme and Peroxidase. *Archives of Oral Biology* **2018**, *89*, 55–64. https://doi.org/10.1016/j.archoralbio.2018.02.007.
(72) Mackle, E. C.; Shapey, J.; Maneas, E.; Saeed, S. R.; Bradford, R.; Ourselin, S.; Vercauteren, T.; Desjardins, A. E. Patient-Specific Polyvinyl Alcohol Phantom Fabrication with Ultrasound and X-Ray Contrast for Brain Tumor Surgery Planning. *JoVE (Journal of Visualized Experiments)* **2020**, No. 161, e61344. https://doi.org/10.3791/61344.
(73) Kim, J.; Kim, I. S.; Cho, T. H.; Lee, K. B.; Hwang, S. J.; Tae, G.; Noh, I.; Lee, S. H.; Park, Y.; Sun, K. Bone Regeneration Using Hyaluronic Acid-Based Hydrogel with Bone Morphogenic Protein-2 and Human Mesenchymal Stem Cells. *Biomaterials* **2007**, *28* (10), 1830–1837. https://doi.org/10.1016/j.biomaterials.2006.11.050.
(74) Kang, C.; Wei, L.; Song, B.; Chen, L.; Liu, J.; Deng, B.; Pan, X.; Shao, L. Involvement of Autophagy in Tantalum Nanoparticle-Induced Osteoblast Proliferation. *Int J Nanomedicine* **2017**, *12*, 4323–4333. https://doi.org/10.2147/IJN.S136281.
(75) Balla, V. K.; Bodhak, S.; Bose, S.; Bandyopadhyay, A. Porous Tantalum Structures for Bone Implants: Fabrication, Mechanical and in Vitro Biological Properties. *Acta Biomaterialia* **2010**, *6* (8), 3349–3359. https://doi.org/10.1016/j.actbio.2010.01.046.
(76) Struffert, T.; Roth, C.; Romeike, B.; Grunwald, I. O.; Reith, W. Onyx in an Experimental Aneurysm Model: Histological and Angiographic Results: Laboratory Investigation. *Journal of Neurosurgery* **2008**, *109* (1), 77–82. https://doi.org/10.3171/JNS/2008/109/7/0077.
(77) Suh, D. C.; Kim, K. S.; Lim, S. M.; Shi, H. B.; Choi, C. G.; Lee, H. K.; Seo, D. M. Technical Feasibility of Embolizing Aneurysms with Glue (n-Butyl 2-Cyanoacrylate): Experimental Study in Rabbits. *AJNR Am J Neuroradiol* **2003**, *24* (8), 1532–1539.
(78) Mao, N.; Gu, T.; Shi, E.; Zhang, G.; Yu, L.; Wang, C. Phenotypic Switching of Vascular Smooth Muscle Cells in Animal Model of Rat Thoracic Aortic Aneurysm. *Interactive CardioVascular and Thoracic Surgery* **2015**, *21* (1), 62–70. https://doi.org/10.1093/icvts/ivv074.

(79) Ji Yadav, S. K.; Vedrtnam, A.; Gunwant, D. Experimental and Numerical Study on Mechanical Behavior and Resistance to Natural Weathering of Sugarcane Leave Reinforced Polymer Composite. *Construction and Building Materials* **2020**, *262*, 120785. https://doi.org/10.1016/j.conbuildmat.2020.120785.
(80) Dong, H.; Russell, D. S.; Litsky, A. S.; Joseph, M. E.; Mo, X.; White, R. D.; Kolipaka, A. In Vivo Aortic Magnetic Resonance Elastography in Abdominal Aortic Aneurysm: A Validation in An Animal Model. *Invest Radiol* **2020**, *55* (7), 463–472. https://doi.org/10.1097/RLI.0000000000000660.
(81) Moláček, J.; Třeška, V.; Kobr, J.; Čertík, B.; Skalický, T.; Kuntscher, V.; Křížková, V. Optimization of the Model of Abdominal Aortic Aneurysm – Experiment in an Animal Model. *JVR* **2009**, *46* (1), 1–5. https://doi.org/10.1159/000135659.
(82) Maynar, M.; Qian, Z.; Hernandez, J.; Sun, F.; DeMiguel, C.; Crisostomo, V.; Usón, J.; Pineda, L.-F.; Espinoza, C. G.; Castañeda, W. R. An Animal Model of Abdominal Aortic Aneurysm Created WithPeritoneal Patch: Technique and Initial Results. *CVIR* **2003**, *26* (2), 168–176. https://doi.org/10.1007/s00270-002-2598-1.